Nano Today 37 (2021) 101095

Contents lists available at ScienceDirect

Nano Today

journal homepage: www.elsevier.com/locate/nanotoday

GMP-grade nanoparticle targeted to nucleolin downregulates tumor molecular signature, blocking growth and invasion, at low systemic exposure

Nuno A. Fonseca[a,b,1], Ana C. Gregório[a,b,1], Vera M. Mendes[a], Rui Lopes[a], Teresa Abreu[a], Nélio Gonçalves[a], Bruno Manadas[a], Manuela Lacerda[c], Paulo Figueiredo[d], Marta Pereira[e], Manuela Gaspar[f], Fabiana Colelli[g], Daniela Pesce[g], Giacomo Signorino[g], Laura Focareta[g], Alessandra Fucci[g], Francesco Cardile[g], Claudio Pisano[g], Tony Cruz[b], Luís Almeida[h], Vera Moura[b], Sérgio Simões[a,i], João N. Moreira[a,i,*]

[a] CNC – Center for Neurosciences and Cell Biology, Center for Innovative Biomedicine and Biotechnology (CIBB), University of Coimbra, Faculty of Medicine (Polo 1), Rua Larga, 3004-504 Coimbra, Portugal
[b] TREAT U, SA, Parque Industrial de Taveiro, Lote 44, 3045-508 Coimbra, Portugal
[c] IPATIMUP - Institute of Molecular Pathology and Immunology, University of Porto, Porto, Portugal
[d] IPOFG-EPE - Portuguese Institute of Oncology Francisco Gentil, Coimbra, Portugal
[e] CHUC – Coimbra's Hospital and University Center, Praceta Prof. Mota Pinto, 3000-075 Portugal
[f] FFUL – Faculty of Pharmacy, University of Lisbon, Av. Prof. Gama Pinto, 1649-003 Lisboa, Portugal
[g] Biogem, Istituto di Biologia e Genetica Molecolare, Via Camporeale, 83031 Ariano Irpino, AV, Italy
[h] Blueclinical, Ltd, Senhora da Hora, 4460-439 Matosinhos, Portugal
[i] UC – University of Coimbra, CIBB, Faculty of Pharmacy, Pólo das Ciências da Saúde, Azinhaga de Santa Comba, 3000-548 Coimbra, Portugal

ARTICLE INFO

Article history:
Received 13 September 2020
Received in revised form 23 December 2020
Accepted 1 February 2021

Keywords:
Nucleolin
Targeted-drug delivery
Mesothelioma
Breast cancer
Nucleolin-overexpressing cancers

ABSTRACT

Patients with breast or ovarian cancer have not benefited from improved efficacy with pegylated liposomal doxorubicin relative to free drug, likely due to the limited extent of the enhanced permeability and retention (EPR) effect, further compromising drug bioavailability in the tumor. Herein it is hypothesized that targeting nucleolin overexpressed in tumor endothelial cells (readily accessible from the vascular compartment), besides cancer cells, with PEGASEMP (doxorubicin hydrochloride in a lipid-based pegylated nanoparticle functionalized with a 31-aminoacid peptide targeting nucleolin), lessens the dependence on high systemic exposures and EPR effect for successful tumor targeting. This strategy has resulted in improved intracellular tumor bioavailability of doxorubicin, at low systemic exposure, associated with a safe toxicological profile. Levels of cell surface nucleolin dictated the antitumor activity of PEGASEMP against nucleolin-overexpressing solid tumors of diverse histological origin, evidencing a significant growth inhibition of malignant mesothelioma over the standard of care. Those observations were paralleled by an impairment of the nucleolin-positive vasculature and downregulation of typically overexpressed genes. Patient stratification based on nucleolin mRNA expression correlated with prognosis and enabled identification of breast and mesothelioma tumors that may potentially benefit from PEGASEMP. Overall, a novel principle of drug delivery is presented with potential therapeutic impact across nucleolin-overexpressing human cancers.

Data Availability: The data that support the findings of this study are available from the corresponding author upon reasonable request.

Introduction

Significant efforts have been taken over the last two decades on the development of nanotechnology-based systems, with approximately two-thirds of its applications focusing on cancer treatment

* Corresponding author at: CNC – Center for Neurosciences and Cell Biology, Center for Innovative Biomedicine and Biotechnology (CIBB), University of Coimbra, Faculty of Medicine (Polo 1), Rua Larga, 3004-504 Coimbra, Portugal.
E-mail address: jmoreira@ff.uc.pt (J.N. Moreira).
[1] Equally contributed to the work.

https://doi.org/10.1016/j.nantod.2021.101095
1748-0132/

[1]. Despite the envisioned potential of nanotechnology [1], the therapeutic benefit of the first approvals of nanomedicine-based strategies resulted from enhanced safety profiles, with only a modest benefit on patient survival [2]. The accessibility of nanomedicines to cancer cells and their ability to diffuse and penetrate the neoplastic mass is compromised by, among other barriers [3], the limited extent of the enhanced permeability and retention (EPR) effect in human tumors, resulting in limited drug bioavailability [4,5]. As the overall efficacy will ultimately rely on drug bioavailability at the tumor and/or at the tumor intracellular level, there is the need to engineer novel mechanisms of drug delivery to overcome the EPR dependency associated with existing clinical-approved nanomedicines [6] and thus get a better access to the tumor microenvironment. This limitation has been recently evidenced with the anti-HER2 antibody-targeted liposomal doxorubicin (codenamed MM-302). Notwithstanding its superior preclinical antitumor activity relative to non-targeted liposomal doxorubicin [7], MM-302 did not show any benefit over the control arms, which included non-liposomal chemotherapy in a phase II study with HER2-positive metastatic breast cancer patients (NCT02213744) [tinyurl.com/y7gyq7xq]. Being the HER2 antigen markedly overexpressed on the surface of cancer cells, MM-302 still depends, in a first level of tumor targeting, on a relevant component of the EPR effect, as the extravasation from tumor leaky vasculature to access its target receptor [8]. In fact, this was addressed on a Nature Materials manuscript upon demonstrating that up to 97% of non-targeted nanoparticles accumulated at the tumor site through a trans-endothelial pathway rather than endothelial gaps [9], thus challenging the EPR-based rationale for nanomedicine development in the oncology setting. Thereby, targeting readily accessible overexpressed markers within the tumor microenvironment that promote cell internalization, combined with efficient intracellular drug release, may enable increased efficacy and safety [6].

Following this rationale, nucleolin, a nucleolar protein involved in nucleic acid metabolism [10], has emerged as a potential target in cancer therapy. Its deregulated expression has been identified in non-small cell lung cancer, gastric cancer and ependymoma as an unfavorable prognostic factor associated with a high risk of relapse and low overall survival [11–13]. In fact, under pathological conditions, nucleolin is responsible for the development of malignant traits, contributing to tumorigenesis, and promoting invasion and angiogenesis [10]. Interestingly, an increased localization of nucleolin at the cell membrane has been identified in both cancer cells and endothelial cells from tumor angiogenic vessels, where the protein modulates the internalization of different ligands as part of the nucleus-cytoplasm-membrane shuttling [14,15].

We have previously demonstrated that pegylated (PEG) liposomes enabling pH-dependent triggered drug (doxorubicin) release, functionalized with a nucleolin-binding F3 peptide, were characterized by a ligand-dependent (*in vitro*) interaction against nucleolin-overexpressing cells and significantly impaired tumor vasculature, reduced the viable tumor area while limiting invasion to surrounding tissues of nucleolin-overexpressing tumors implanted in the mammary fat pad (relative to non-targeted counterpart and free drug) [16]. Based on these observations, we hypothesized that *in vivo* targeting of nucleolin overexpressed at the readily accessible (upon intravenous administration) surface of endothelial cells from tumor vasculature, besides cancer cells, would facilitate the access of nucleolin-targeting nanoparticles to the microenvironment of solid tumors, thus lessening the dependence on the EPR effect. This would improve overall intracellular delivery efficiency, and therefore, enhance the bioavailability of the encapsulated payload at the tumor level relative to a long circulating nanoparticle devoided of ligand-mediated targeting. To test this hypothesis, pH-sensitive liposomes containing doxorubicin and functionalized at the PEG extremity with the nucleolin-binding F3 peptide (codenamed PEGASEMP) were engineered and manufactured under *Good Manufacturing Practices* (GMP). Herein, the nucleolin-dependent antitumor effect of PEGASEMP against different animal models of cancer is described. Enhanced cytosolic delivery of doxorubicin was evidenced, at the tumor level, while maintaining a significantly (and surprisingly) lower systemic exposure and safer toxicological profile, compared to Caelyx, upon intravenous administration. Downregulation of tumor invasion and transcripts associated with cell division machinery further contributed to the significant antitumor effect of PEGASEMP in murine models of mesothelioma. Overall, these observations support a novel principle of drug delivery towards solid tumors, with potential therapeutic impact across nucleolin-overexpressing cancers.

Results

Physical characterization of pH-sensitive and nucleolin-targeting GMP-grade pegylated liposomes

The GMP-grade batch used herein was developed based on a previous described formulation of doxorubicin-loaded pH-sensitive pegylated liposomes targeted to nucleolin [16], and codenamed PEGASEMP (Fig. 1a, b). The nucleolin targeting component was incorporated by formulating the liposomes for the first time in the presence of a novel custom synthetic entity produced by covalently linking DSPE-PEG_{2k} and F3 peptide through a 6-atom spacer (DSPE-PEG_{2k}-F3, Fig. 1c). The potency of the sterile formulation was adjusted to 2 mg of doxorubicin *per* mL (drug loading 0.18:1 [doxorubicin:total lipid]). Characterization by electron microscopy (TEM) demonstrated that PEGASEMP presented spherical shape with an electron-opaque core, absent in empty PEGASEMP, but similar to Caelyx (Fig. 1d). Measurements of electron imaging indicated that PEGASEMP presented a median size of 78.9 nm [59.1^{25th}-96.1^{75th} nm], consistent with the dynamic light scattering (DLS) observation of a monodispersed mean size of 91.2 nm (polydispersion index of 0.036 ± 0.006) (Fig. 1d–f). Those characteristics were comparable to the data acquired for Caelyx (TEM: 103.6 nm [92.1^{25th}-114.7^{75th} nm]; DLS: 86.8 nm (polydispersion index of 0.027 ± 0.004)) or the empty counterpart of PEGASEMP (TEM: 87.7 nm [76.6^{25th}-100.3^{75th} nm]; DLS: 90.7 nm (polydispersion index of 0.059 ± 0.005)) (Fig. 1d–f). Furthermore, PEGASEMP's (and its empty *counterpart*) zeta potential differed from Caelyx's (+ 4.9 ± 0.2 mV and + 6.2 ± 0.2 mV *versus* + 0.2 ± 0.3 mV) (Fig. 1f). Importantly, the above observations (at 0 h) were generically maintained after storing each formulation at 5 ± 3 °C for 72 h, except for a slight increase in the mean size of empty PEGASEMP observed by TEM (Fig. 1d, f). Longer stability studies at 5 ± 3 °C indicated that PEGASEMP's lipid and doxorubicin content, as well as physical (mean size and drug retention) and functional (*in vitro* drug delivery) characteristics, were stable for at least 3 months (Fig. 1g). In the presence of serum or mouse blood, PEGASEMP presented a similar release profile (Fig. S1a) and recovery of doxorubicin (preventing drug partitioning into red blood cell compartment [17,18]) (Fig. S1b), respectively, as compared to Caelyx, altogether indications of identical *in vivo* stability.

Overall, PEGASEMP presented adequate characteristics (that remained stable overtime) for intravenous administration and, in the most relevant aspects, comparable to Caelyx.

Toxicokinetic assessment of PEGASEMP in rats and beagle dogs demonstrates overall favorable tolerability versus Caelyx

Toxicological assessment was performed in superior species (rats and dogs, Fig. 2a) using experimental designs that established Caelyx's preclinical toxicity and pharmacokinetic profiles [19].

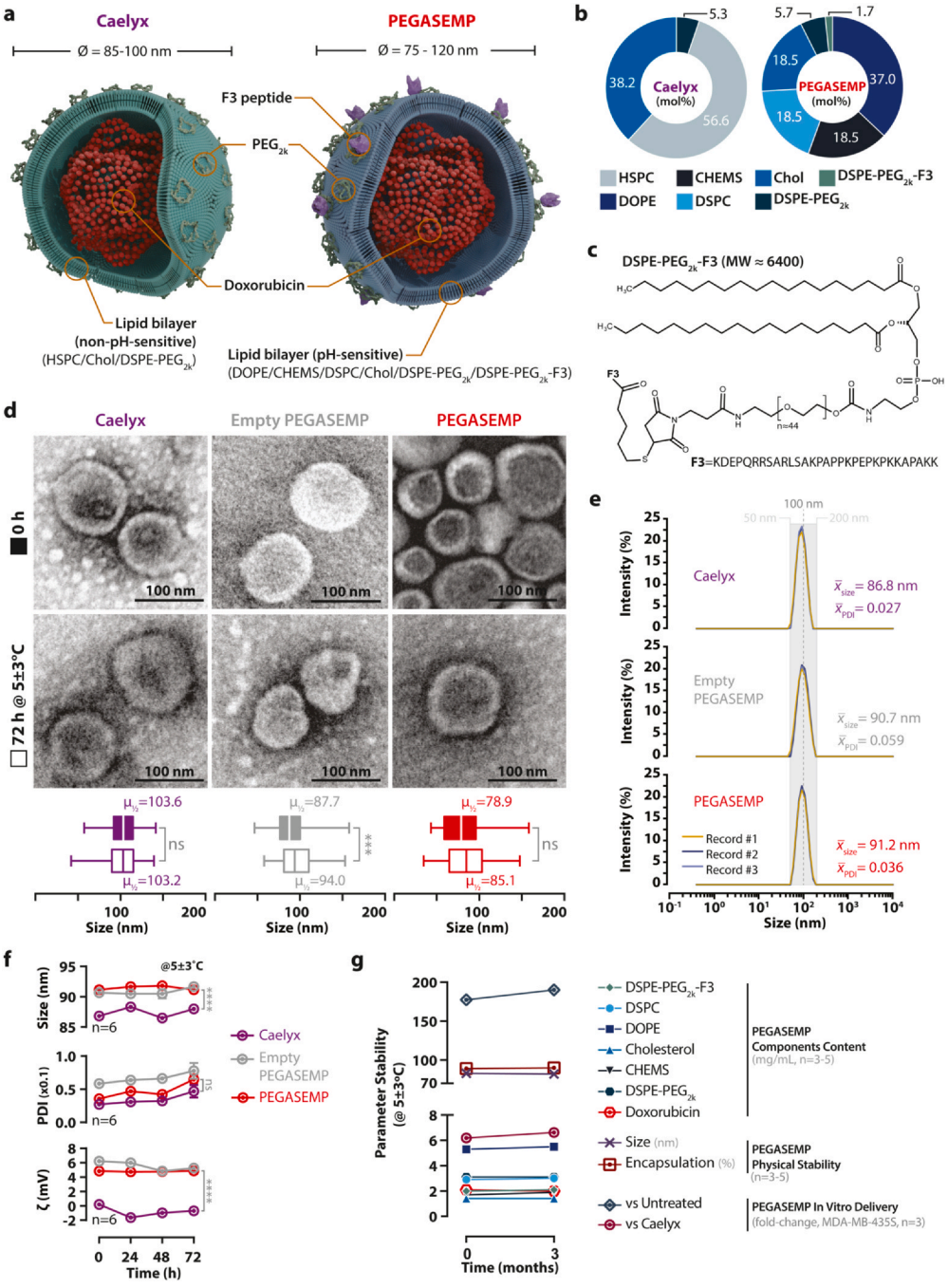

Fig. 1. PEGASEMP's structure and characterization. (a) Schematic representation of PEGASEMP characteristics in comparison with Caelyx. Size specification for both formulations is shown. (b) Relative composition (mol%) of the lipid bilayer of PEGASEMP and Caelyx. (c) Molecular structure of the synthetic DSPE-PEG$_{2k}$-F3 peptide conjugate. (d) Representative microphotographs of structural morphology (transmission electron microscopy) and size distribution analysis of PEGASEMP, performed before (0 h) and after 72 h at 5 ± 3 °C. Caelyx and empty version of PEGASEMP were used as controls. Data are represented as the minimum to maximum liposomal size distribution, with the box width and the line (inside the box) representing 25th-75th percentile interval and median ($\mu_{½}$), respectively (p-values calculated with Mann-Whitney test, n = 119–172). (e) Representative intensity-weighted (%) dynamic light scattering histograms (3 records) of PEGASEMP, compared to Caelyx and empty PEGASEMP. The mean ($\bar{x}$) size and polydispersion index (PDI) values are presented. (f) Time-lapse analysis of size, polydispersion index and zeta potential (ζ) upon storage of each formulation at 5 ± 3 °C (p-values calculated with Tukey's multicomparison test at 72 h, n = 6). (g) Long-term stability of PEGASEMP's lipid and doxorubicin contents, mean size, drug encapsulation and *in vitro* drug delivery (assessed with MDA-MB-435S cells). Each data point represents the mean value (n = 3–5). ^{ns} p > 0.05, *** p < 0.001, ****p < 0.0001. DOPE: 2-dioleoyl-sn-glycero-3-phosphoethanolamine; CHEMS: 3β-hydroxy-5-cholestene-3-hemisuccinate; DSPC: 1,2-distearoyl-sn-glycero-3-phosphocholine; HSPC: L-α-phosphatidylcholine, hydrogenated (Soy); Chol: cholesterol; DSPE-PEG$_{2k}$: 1,2-distearoyl-sn-glycero-3-phosphoethanolamine-N-[methoxy(polyethylene glycol)−2000]; DSPE-PEG$_{2k}$-F3: 1,2-distearoyl-sn-glycero-3-phosphoethanolamine-N-[methoxy(polyethylene glycol)−2000]-F3 peptide.

Regardless gender, in rats (Fig. 2b) and dogs (Fig. 2c), PEGASEMP enabled, surprisingly, a systemic exposure of doxorubicin, at least, 7.8-fold lower than the one enabled by Caelyx (Fig. 2b, c). Notwithstanding PEGASEMP impact in rat body weight relative to saline (Fig. 2d), as a general indication of toxicity, in both species it demonstrated a lower impact on body weight variation as compared to Caelyx, despite overall gender differences (Fig. 2d, e). The latter has caused a decrease of the mean relative body weight that was equal or higher than 10% in male or female dogs, respectively (Fig. 2e). Moreover, the absence of significant impact on body weight

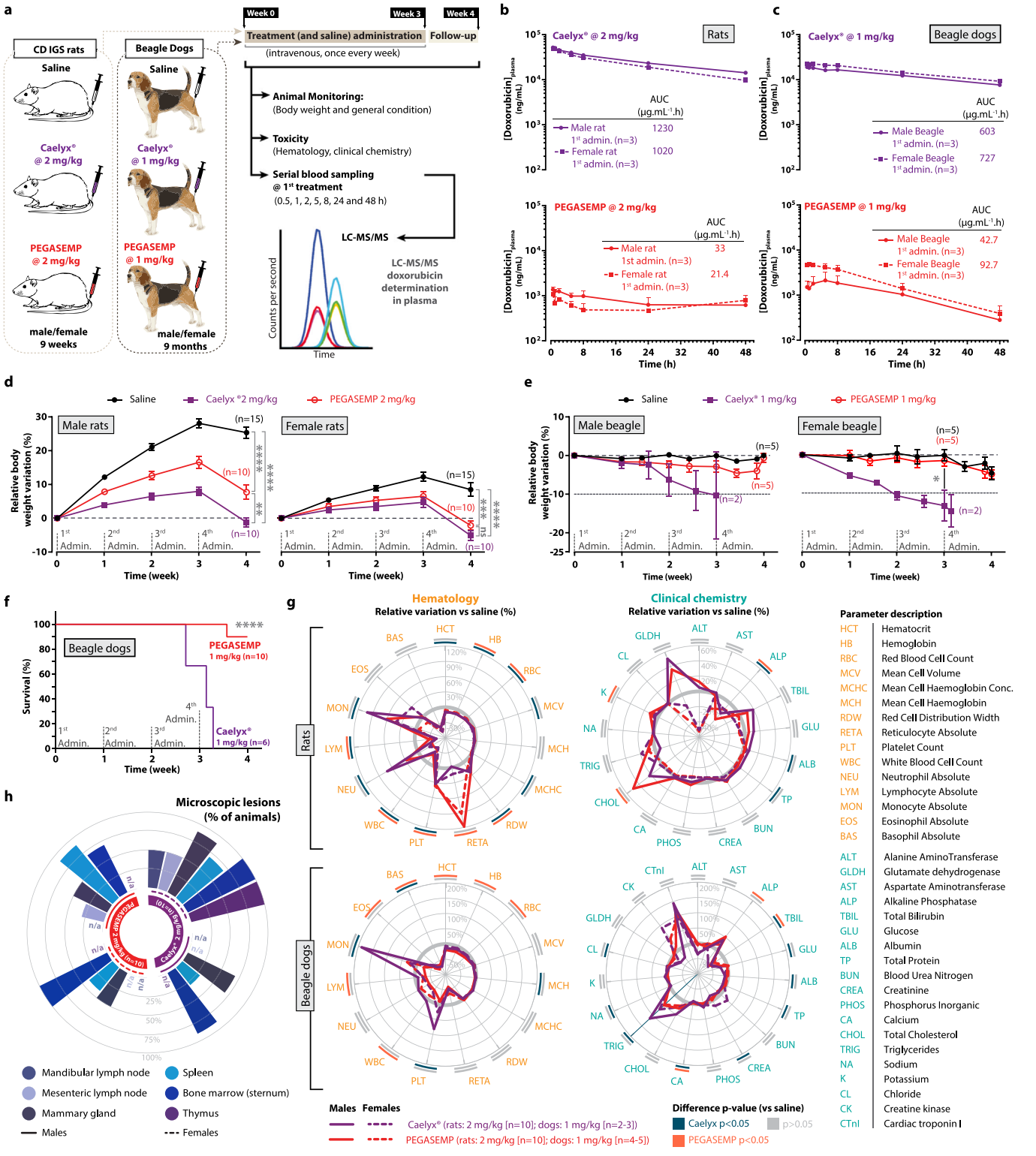

Fig. 2. PEGASEMP toxicokinetic assessment in rats and beagle dogs. (a) Evaluation of PEGASEMP pharmacokinetic and toxicological profile in rats and dogs. PEGASEMP was weekly administered i.v. to CD IGS® rats and beagle dogs, at indicated doxorubicin doses (4 weeks). Caelyx was used as a control. Serial blood sampling was performed at indicated timepoints (first treatment) for doxorubicin quantification in the plasma. Further blood collection enabled the assessment of clinical chemistry and hematological parameters. (b, c) Doxorubicin plasma profile in rats and dogs upon single administration of PEGASEMP or Caelyx, at indicated doses. Each timepoint represent the mean of doxorubicin plasma concentration (± SEM, n = 2–3). Insert tables refer to the respective area under the curve (AUC). (d, e) Relative body weight variation of rats and dogs, respectively (rats: p-values calculated with Tukeys's test at week 4, n = 10–15; dogs: p-value calculated with Dunn's test at week 3, n = 2–5). (f) Survival of dogs administered with PEGASEMP or Caelyx, in equimolar doses of doxorubicin (n = 6–10, p-value calculated with logrank test). (g) Mean relative variation (%; *versus* saline) of hematological and clinical chemistry parameters of rats (at week 4; n = 10) and dogs (at week 3, except for cardiac troponin, measured at week 2; n = 2–5); difference p-value is graphically indicated by the outer rim tags. Inner bold circle represents the saline baseline. *For mean differences and p-values see* Tables S1–S4. (h) Percentage of rats with microscopic lesions upon histological analysis of indicated organs, at week 4 (n = 10). ^{ns} p > 0.05, *p < 0.05, **p < 0.01, ***p < 0.001, ****p < 0.0001.

evidenced by PEGASEMP-treated group (Fig. 2e), correlated with a better survival of animals as compared to Caelyx-treated group, at the same dose and administration schedule (Fig. 2f). Empty PEGASEMP demonstrated no or residual impact on body weight (in rats and dogs, respectively; Fig. S2) and on hematological/chemistry parameters (not shown), relative to saline.

In rats, PEGASEMP and Caelyx induced a decrease in lymphocytes (or overall white blood cells and basophils) as compared to the saline control (Fig. 2g). The impact of PEGASEMP over remaining hematological parameters was, in general, identical to Caelyx, with variations occurring near or within normal range values (Fig. 2g and Table S1) [20–22]. Exceptionally, reticulocyte count was increased for animals (both males and females) administered with PEGASEMP (Fig. 2g), normally associated with regenerative anemia [20]. Nevertheless, only a marginal decrease in red blood cells was observed (Fig. 2g and Table S1). In dogs, PEGASEMP and Caelyx were associated with minimal decreases in hematocrit, hemoglobin, red blood cells, reticulocyte count, white blood cells (females) and lymphocytes (still within normal value range) (Fig. 2g and Table S2). In both species, PEGASEMP had no relevant impact over clinical chemistry parameters, similarly to Caelyx (Fig. 2g and Tables S3, S4). In dogs, an increase (within normal values) in cardiac Troponin I was observed in animals from both treatment groups relative to saline (Fig. 2g and Table S4).

Furthermore, PEGASEMP evidenced an overall lower incidence of microscopic lesions in relevant female rat tissues as compared to Caelyx, less evident in the case of males (Fig. 2h). In dogs, PEGASEMP and Caelyx related microscopic alterations were identified in lymphocyte maturation organs (sternum-bone marrow, thymus, spleen and mandibular and mesenteric lymph nodes), and testes (deletion of germ cells), overall accompanied by organ weight loss in testes and thymus (the latter in a higher extent for Caelyx) (Fig. S3 and Tables S5, S6). The severe alterations in the skin and digestive system observed for the Caelyx group (as also previously described [19]), relative to PEGASEMP, were associated with decreased food consumption in male rats from the former group (Fig. S4 and Table S7).

Overall, delivery of doxorubicin by a nanoparticle functionalized with a nucleolin-binding peptide, as PEGASEMP, presented fewer debilitating effects (including over clinical chemistry and hematology parameters) than a strategy based on the delivery of the same drug through a non-targeted and non-pH-sensitive formulation, thus supporting a better tolerability of PEGASEMP as compared to Caelyx.

Nucleolin targeting overrides EPR-driven tumor accumulation enabling high extent intracellular delivery of doxorubicin and antitumor activity of PEGASEMP

The previous toxicokinetic assessment supported a higher tolerability of PEGASEMP relative to Caelyx, likely due to the lower systemic exposure of doxorubicin associated with the former. These data led us to assess the therapeutic activity at equitoxic doses, recovering the MDA-MB-435S tumor model (Fig. 3a) previously used [16]. Despite its reclassification [23,24], MDA-MB-435S cells enable the development of nucleolin-overexpressing tumors (nucleolin^{high}), as compared to other cells lines [16], within any relevant environment, including the mammary fat pad, essential to the study of moieties targeting nucleolin, as the case of the F3 peptide, as previously performed by others [14]. Accordingly, female BALB/c$^{nu/nu}$ mice, bearing nucleolin^{high} MDA-MB-435S tumors, were treated with PEGASEMP at 7 mg of doxorubicin/kg, the dose equivalent to 1 mg/kg in dogs (Fig. 2f) [25], once a week for five weeks (Fig. 3a) (cumulative dose of 35 mg/kg), in line with safety observations above (Fig. 2f). Caelyx, the EPR gold-standard, was used as control at a cumulative dose of 25 mg/kg (divided in 5 administrations, one every week), the known maximum tolerated dose against different human xenograft tumors derived in nude mice, contrary to the cumulative dose of 36 mg/kg [19,26]. It was initially confirmed in mice that the mean systemic exposure of doxorubicin, as assessed by the area under the curve ($AUC_{5min\text{-}24h}$) of plasma concentrations, delivered by PEGASEMP (at 7 mg/kg) was 4.7-fold lower than the one observed for Caelyx (at 5 mg/kg) (Fig. 3b), in line with the observation in rats and dogs (Fig. 2b, c).

Notwithstanding the differences in AUC, the treatment with PEGASEMP and Caelyx enabled a similar impact in terms of reduction of tumor burden in animals bearing nucleolin^{high} MDA-MB-435S tumors (Fig. 3b). Furthermore, PEGASEMP improved overall survival by 37% for animals bearing nucleolin^{high} MDA-MB-435S tumors relative to Caelyx-treated mice (Fig. 3b), with equitoxic impact in body weight (less than 10% loss of body weight within the timeframe of the study) (Fig. S5). Further stereology-based [27] histological analysis of nucleolin^{high} MDA-MB-435S tumors of animals that completed the scheduled treatment (Fig. 3a), demonstrated that PEGASEMP, at 7 mg/kg, decreased by 19-fold the area of nucleolin^{+} tumor vasculature relative to Caelyx, with a lower impact on the CD31^{+} mature vasculature [28] (Fig. 3b, c). Supporting these observations, PEGASEMP's tumor bioavailability index (number of doxorubicin^{+} cells *per* field, evaluated by confocal microscopy (Fig. 3d), normalized to the systemic exposure [$AUC_{5min\text{-}24h}$]), accounting the actual circulating liposomal doxorubicin becoming bioavailable was 10.8-fold higher than the one enabled by Caelyx (Fig. 3b, d). Simultaneously, tumor delivery index, as measured by the bulk amount of doxorubicin in the tumor, assessed by liquid-chromatography tandem mass spectrometry and normalized to the systemic exposure [$AUC_{5\ min\text{-}24\ h}$], remained essentially the same for both formulations (Fig. 3b).

Importantly, in a breast cancer model derived from 4T1 cells (nucleolin^{low}), expressing 2.3-fold lower cell surface nucleolin relative to MDA-MB-435S cells (associated with lower extent of internalization, Fig. S6a, b) but yet more sensitive to doxorubicin delivered by PEGASEMP *in vitro* (Fig. S6c), the latter had a residual impact on tumor burden or animal survival (Fig. S6d–g) at any dose tested. Supporting the targeting specificity of the F3 peptide, it was further shown that it promoted (in the form of DSPE-PEG_{2k}-F3 micelles) cell surface nucleolin clustering (Fig. 3e) with a 3-fold increase in cell surface levels relative to untreated cells (Fig. 3f, g). This nucleolin-dependent effect was further confirmed, as the cell surface levels of proteins like neuropilin-1 (involved in the internalization of peptides with CendR sequences [29]) and CD44 (a glycoprotein, like nucleolin, highly expressed in cancer cells [30]) did not change in the presence of the F3 peptide (Fig. 3g), without an impact on the total nucleolin expression (Fig. 3h). Furthermore, it was shown that the high extent cellular association of F3 peptide-targeted liposomes could be significantly decreased upon incubation with tunicamycin (Fig. 3i), a N-glycosylation inhibitor that blocks nucleolin translocation to the cell surface [31].

Collectively, the results supported a nucleolin-dependent antitumor effect, subsequent to the improved intratumor bioavailability of doxorubicin delivered by PEGASEMP, under a safer toxicological profile, promoted by its lower systemic exposure, relative to a formulation as Caelyx (Fig. S7), which main of mechanism of action relies on the EPR effect.

PEGASEMP's enables significant mesothelioma growth inhibition relative to the standard-of-care

Owing to the proposed mechanism of action of PEGASEMP, and its payload, it was important to assess its antitumor activity on a cancer model with a molecular signature strongly associated with cell division. In this respect [32], mesothelioma is a highly metastatic cancer, with poor prognosis, affecting the mesothelium upon asbestos exposure [33], that overexpresses nucleolin (Fig. 4a). Accordingly, the therapeutic activity of PEGASEMP was evaluated

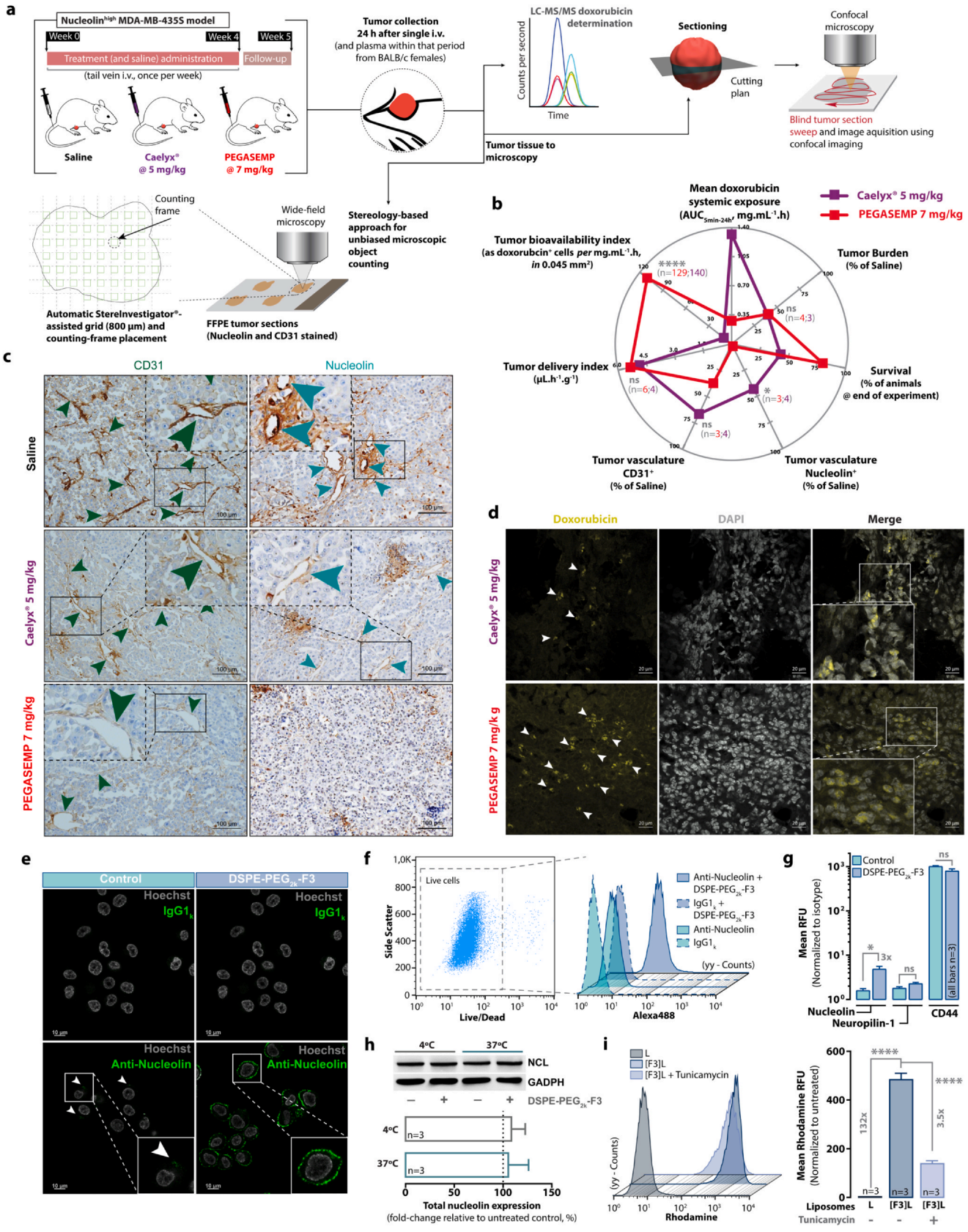

(caption on next page)

Fig. 3. Nucleolin-mediated intracellular delivery underlying the antitumor effect of PEGASEMP at low mean systemic exposure of doxorubicin. (a) Experimental design. PEGASEMP (pH-sensitive liposomal doxorubicin functionalized with F3 peptide-binding nucleolin) was weekly administered i.v. (for 5 weeks) to female BALB/$c^{nu/nu}$ mice bearing nucleolin high MDA-MB-435S mammary tumors. Caelyx and saline solution (same schedule) were used as controls. Animal monitoring and a stereology-based approach for unbiased microscopic object counting (area of nucleolin$^+$/CD31$^+$ vessels in tumor sections) was performed. In a different set of animals, assessment of doxorubicin tumor accumulation (24 h after administration) and plasma clearance profile (in BALB/c mice) was performed, following intravenous administration of PEGASEMP (*versus* Caelyx); tumors were harvested 24 h after administration or blood was collected up to 24 h, two bleeds *per* animal, respectively. (b) Radial plot integrating data on efficacy (tumor burden [n = 3–4, end of experiment], survival [n = 5–7] and impact on CD31$^+$/nucleolin$^+$ vasculature [n = 3–4, p-value calculated with *t*-test]) and pharmacokinetics (mean doxorubicin systemic exposure [$AUC_{5min-24h}$, n = 3–4], tumor delivery index [n = 4–6, p-value calculated with Mann-Whitney test] and bioavailability index [n = 129–140 images, p-value calculated with Mann-Whitney test]) of doxorubicin delivered by PEGASEMP and Caelyx. (c) Microphotographs (20x) of CD31 (green arrows) and nucleolin (blue arrows) stained MDA-MB-435S tumor sections of animals that have undergone 5 treatments. Scale bar = 100 µm. (d) Representative laser confocal images (40x) of intratumoral doxorubicin fluorescence. Scale bar = 20 µm. (e) Confocal live cell imaging of MDA-MB-435S cells incubated with DSPE-PEG_{2k}-F3 peptide micelles and anti-NCL-Alexa®488 (green) antibody (or the IgG_{1k} isotype control) at 4 ºC for 15 min. Scale bar = 10 µm. (f) Representative flow cytometry histograms of live MDA-MB-435S cells upon incubation with DSPE-PEG_{2k}-F3 peptide micelles and anti-NCL-Alexa®488 antibody or corresponding controls for 60 min at 4 °C. (g) Impact of DSPE-PEG_{2k}-F3 peptide micelles in cell surface expression levels of nucleolin, neuropilin-1 (NRP1) and CD44 measured by flow cytometry. Data present the mean ± SEM (n = 3, p-values calculated with unpaired *t*-test). (h) NCL protein density (from total extracts) upon incubation of MDA-MB-435S cells with DSPE-PEG_{2k}-F3 peptide micelles for 60 min at 4 °C or 37 °C. Data represent the mean ± SEM (n = 3, p-value calculated with unpaired *t*-test). (i) Cellular association of F3 peptide-targeted liposomes ([F3]L), fluorescently labeled with rhodamine, after culturing MDA-MB-435S cells in the presence or absence of tunicamycin, an inhibitor of N-glycosylation. Data represent the mean ± SEM (n = 3, p-value calculated with Tukey's multicomparison test). $^{ns}p > 0.05$; $^{*}p < 0.05$; $^{****}p < 0.0001$. (For interpretation of the references to color in this figure legend, the reader is referred to the web version of this article.)

against orthotopic animal models of different sub-types of human mesothelioma, established in female CD-$1^{nu/nu}$ mice: the highest incidence epithelioid subtype (derived from MM473:Luc cells), and the most aggressive biphasic subtype (derived from MM487:Luc cells). In the latter, animals were treated at an early stage and advanced stage of disease progression (Fig. S8), recapitulating the different stages of tumor development in patients, at diagnosis (Fig. 4b).

In the epithelioid mesothelioma model, treatment with PEGASEMP at 7.0 mg/kg (q7dx5) enabled a tumor growth inhibition of 209- or 55-fold, relative to non-treated mice or treated with the standard of care (combination of cisplatin [4 mg/kg, q7dx5] and pemetrexed [100 mg/kg, q2dx3×5] [33]), respectively (Fig. 4c). A similar trend was observed with PEGASEMP at 5.6 mg/kg, alone or in combination with cisplatin, but in a lower extent than at 7.0 mg/kg (20.2- or 25.2-fold difference in the BLI mean signal relative to non-treated mice, at day 42, respectively) (Fig. 4c). The combined treatment with cisplatin and pemetrexed presented a limited effect on tumor growth, relative to the non-treated animals (administered with saline) (Fig. 4c). A similar result was observed with cisplatin alone (Fig. 4c). None of the treatments tested enabled any toxic effect, as illustrated by the variation of the animals' body weight over time (Fig. 4d).

Regarding the biphasic subtype, at the early stage of tumor development, treatment with PEGASEMP, at 7.0 mg/kg, presented the highest efficacy in tumor growth inhibition relative to the standard of care combination, where a 2713-fold difference was observed (Fig. 4e). At the advanced stage of development, the combination of PEGASEMP and cisplatin was the most active, inhibiting tumor growth by 107-fold relative to standard-of-care (Fig. 4e). However, PEGASEMP as monotherapy did not depart significantly from the standard of care (Fig. 4e). In both stages, animals did not evidence body weight loss over time (Fig. 4f), in spite of PEGASEMP/cisplatin combination hindered body weight gain relative to PEGASEMP alone, although without statistical significance (Fig. 4f).

PEGASEMP decreases mesothelioma tumor burden and limits invasion to surrounding organs

The overall tumor growth inhibition enabled by PEGASEMP at 7 mg/kg, translated into a significant reduction of tumor burden in the epithelioid and (early-stage) biphasic animal models, relative to the standard-of-care (79- or 1223-fold for MM473:Luc or MM487:Luc at early stage, respectively) (Fig. 4g–i). In the case of the biphasic advanced-stage model (MM:487:Luc Advanced stage), the combination of PEGASEMP at 5.6 mg/kg with cisplatin enabled the highest reduction in tumor burden relative to the standard-of-care (55-fold difference) (Fig. 4i). Overall, treatment with the standard of care did not show any effect on tumor burden across the different mesothelioma sub-types tested (Fig. 4g–i).

Importantly, animals bearing epithelioid tumors and treated with PEGASEMP either at 7.0 or 5.6 mg/kg (combined with cisplatin) presented the lowest incidence of tumor infiltration into the chest cavity (57.1% and 50%, respectively), as compared to the standard-of-care-treated group, in which all animals presented infiltrations (Fig. 4j). Those results correlated with the high extent of "none to slight" lung neoplastic lesions associated with PEGASEMP alone at 7 mg/kg, or combined with cisplatin (57.1% or 62.5%, respectively), in contrast with the 12.5% from standard-of-care ("mild to marked" lesions reached an extent of 87.5%) (Fig. 4k, l).

PEGASEMP downregulates cell division-associated transcriptome of mesothelioma

Aiming at understanding the transcriptome alterations underlying the antitumor effect of PEGASEMP, orthotopic mesothelioma tumors (at advanced stage) were harvested from animals treated twice with PEGASEMP at 7 mg/kg/week, schedule that guaranteed enough material for further transcriptomic microarray analysis (Fig. 5a). According to the established parameters for differential gene expression analysis (Fig. S9), 146 gene transcripts were found to be deregulated (Fig. 5b, Table S8). Of those, 75% were downregulated while the remaining 25% were upregulated (Fig. 5b). Gene ontology analysis of the differentially expressed genes demonstrated that the most relevant altered processes (FDR < 0.001, PANTHER Biological Process GO-Slim database) involved the downregulation of cell division, including cell cycle or chromatin organization and assembly (Fig. 5c, Table S9). Further comparison against the PANTHER Cell Component GO-Slim database confirmed those observations, by linking with cell components such as chromosomes, microtubules or DNA-protein complexes (Fig. S10, Table S10). Furthermore, differentially expressed genes (mapped against PANTHER database) formed a relevant interaction network (protein-protein enrichment p-value $< 1.0 \times 10^{-16}$) as *per* STRING analysis, with proteins such as aurora kinase, cyclin B1, polo-like kinase 1 or topoisomerase 2 A (AURKA, CCNB1, PLK1, TOP2A, respectively) as a part of a cell cycle regulatory cluster sided by a large histone cluster (Fig. 5d). Significantly, data demonstrated that PEGASEMP generically downregulated part of the 50 gene transcripts consensually described as overexpressed in malignant mesothelioma [32] (Fig. 5e, Tables S11, S12). In fact, and only upon two treatments, 14% of those fitted the differential expression criteria, and included the downregulation of transcripts encoding topoisomerase 2, cyclin B1 or the proliferation marker Ki67 (TOP2A, CCNB1 or MKI67, respectively) (Fig. 5e). Interestingly, transcripts encoding P53 Inducible Nuclear Protein 1 (antiproliferative and pro-apoptotic protein, positive regulator of autophagy and p53 [34]), MDM2 proto-oncogene (p53-controlled

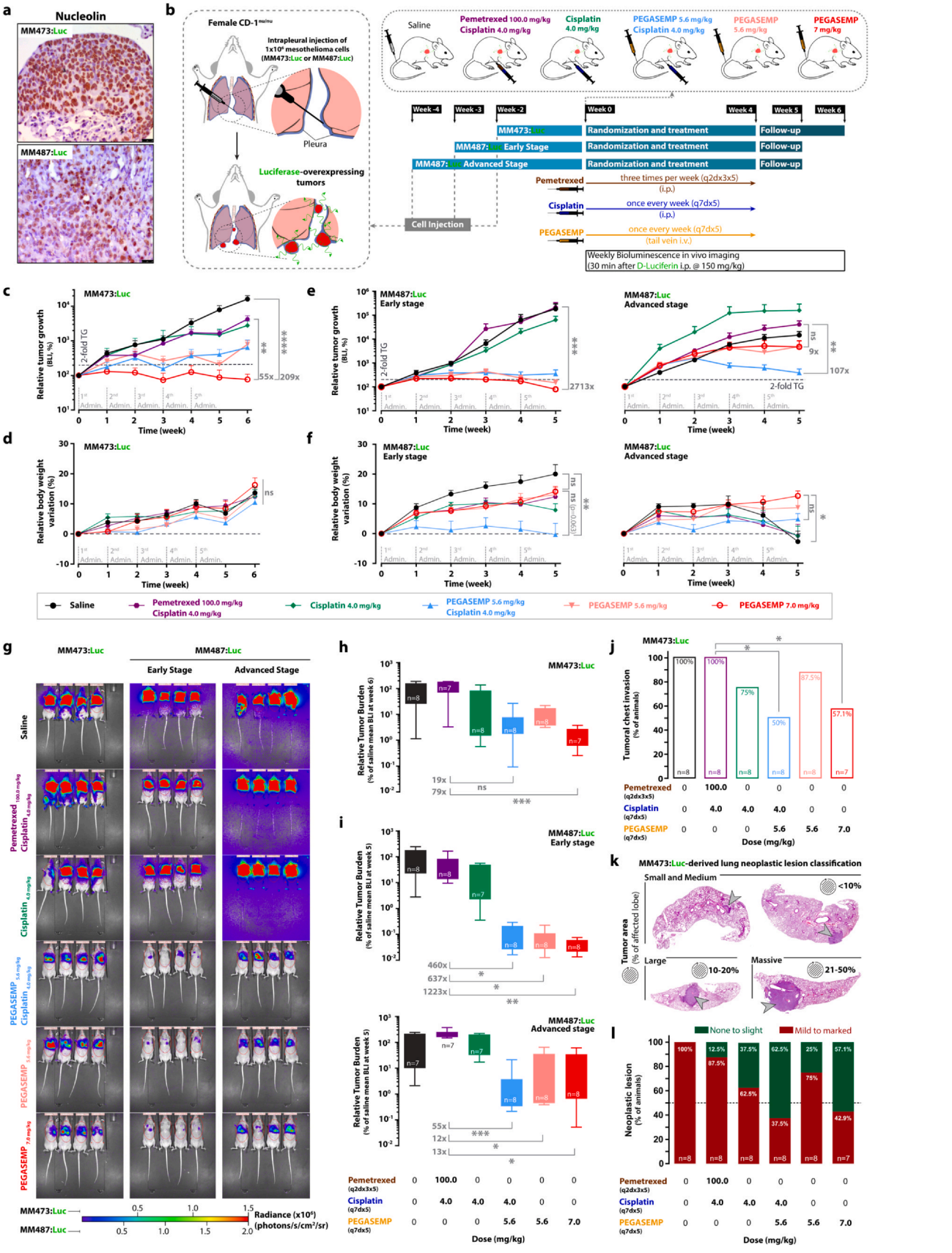

(caption on next page)

Fig. 4. PEGASEMP enables significant growth inhibition of epithelioid and biphasic mesothelioma orthotopic tumors. (a) Microphotographs from nucleolin-stained sections of tumors derived from MM473:Luc epithelioid and MM487:Luc biphasic mesothelioma cells (scale bar = 25 μm). (b) Experimental design of assessment of efficacy of PEGASEMP against epithelioid (MM473:Luc) and biphasic (MM487:Luc, at Early and Advanced stages) murine (female CD-1$^{nu/nu}$ mice) models of human mesothelioma. At week 0, animals were randomly allocated to different treatment groups as indicated. Bioluminescence (BLI, a measure of tumor growth) and body condition were assessed at least once-a-week. (c) Relative tumor growth and (d) mean relative body weight (normalized to treatment start) of animals bearing MM473:Luc mesothelioma tumors. Timepoints represent mean ± SEM (p-values calculated using Dunn's test, n = 7–8). (e) Relative tumor growth and (f) mean relative body weight (normalized to treatment start) of animals bearing MM487:Luc mesothelioma (Early or Advanced stage) tumors. Timepoints represent mean ± SEM (p-values calculated using Dunn's test, n = 7–8). (g) Representative bioluminescence images of animals bearing MM473:Luc and MM487:Luc-derived tumors at the end of the experiment (week 6 and week 5, after start of treatment start, respectively). (h) MM473:Luc and (i) MM487:Luc tumor burden at the end of the experiment (p-values were calculated by Dunn's test). (j) Assessment of chest invasion in animals with MM473:Luc tumors, detectable at necropsy (p-value calculated using χ^2 test, n = 7–8). (k) Scans of lung H&E sections of animals bearing MM473:Luc tumors exhibiting pulmonary lesions (arrows) with different levels of severity. (l) Animals (%) with neoplastic lesions in the lungs, according to severity (n = 7–8). *See Materials and Methods section* for severity classification. TG – tumor growth. ^{ns} p > 0.05, *p < 0.05, **p < 0.01, ***p < 0.001, ****p < 0.0001.

transcription under stress conditions [35,36]), collagen 1 and Fibroblast Growth Factor 2 (TP53INP1, MDM2, COL1A2 and FGF2, respectively) were upregulated (Fig. 5c).

Altogether, both relevant down and upregulated transcripts were consistent with cell cycle arrest and cell death.

Nucleolin-based breast cancer and mesothelioma patient stratification identifies biologically distinct tumors susceptible to benefit from PEGASEMP

Previous data analysis has shown that nucleolin mRNA expression identifies breast tumors with different prognosis and gene expression profiles [37]. Thus, breast cancer (GSE7390 and GSE2034 [n = 198 and 286, respectively]) and mesothelioma (GSE2549, n = 45) datasets [38–40] were explored to define the clinical value of nucleolin in the context of PEGASEMP-based therapeutic intervention. In fact, high expression level of nucleolin in breast cancer was associated with increased disease-free survival (Fig. 6a), while low expressing tumors (nucleolin^{low}) exhibited a poorer prognosis in line with previous observations [37]. Moreover, the nucleolin-overexpressing groups (nucleolin^{high}) from both breast cancer datasets presented, at least, 1.9-fold (p < 0.03) enrichment of estrogen receptor-negative (ER-) breast tumors relative to nucleolin^{low} tumors (Fig. 6b).

In agreement with those observations, nucleolin^{low} mesotheliomas presented poorer overall survival (Fig. 6c), while the nucleolin^{high} group was enriched for the epithelial mesothelioma subtype (Fig. 6c, insert) and presented 1.35-fold higher nucleolin mRNA levels (p = 0.007) relative to normal pleura tissue (Fig. 6d). Interestingly, clustering (Fig. 6e) and differential gene expression analysis (Fig. 6f) demonstrated that nucleolin^{high} and nucleolin^{low} mesotheliomas differ in terms of genetic signature (even compared to normal pleura). In fact, cluster 2 and 7 presented, approximately, 15% and 9% differently expressed genes (p-value < 0.05) (Fig. 6f, insert), which were related to the upregulation of nucleic acid processing and metabolic functions in nucleolin^{high} mesotheliomas (Fig. 6g). Thus, this suggested that nucleolin^{high} mesotheliomas are biologically different from nucleolin^{low} tumors, as previously suggested in breast cancer [37], and potentially more sensitive to PEGASEMP, from the point of view of nucleolin targeting and activity of antiproliferative activity of a payload as doxorubicin.

Discussion

Currently clinically available nanoparticles have had a major impact on improving the safety profile of conventional chemotherapy (namely doxorubicin) [41]. However, it has been demonstrated that less than 1% of the (intravenously) administered dose of a given nanoparticle, regardless of its nature, accumulates at the tumor site [42]. This is associated with the absorption, distribution, metabolism and excretion (ADME) processes affecting nanoparticles (either ligand-mediated targeted or non-targeted) as any other xenobiotic, although at different extents [3,42,43]. If one accounts both the marked extent of retention of nanoparticles in the liver and the limited extent of the EPR effect in patients, owed to patient-derived tumor heterogeneity, it becomes apparent that drug bioavailability at tumor/cell level is strongly impaired, with a negative impact on efficacy [5,6]. Thus, shifting from the exclusive *cancer cell-targeting* paradigm towards exploiting additional readily accessible overexpressed markers, including on the tumor vasculature, with simultaneous combination with intracellular triggered (burst) drug release, could lessen the dependence on EPR to achieve therapeutic efficacy against solid tumors [6]. This has been emphasized by the recent demonstration that the endothelial fenestrations are not the major entry pathway of nanoparticles into solid tumors, but rather active processes through endothelial cells [9]. This could have a positive impact on the overall pharmacodynamic of triggered drug release formulations, as pH-sensitive liposomes based on DOPE and CHEMS, have been limited by their short blood circulation half-lives [44,45], and thus low systemic exposure.

Accordingly, we aimed at addressing the question on whether nucleolin targeting could enable a (GMP-grade) pH-sensitive liposomal formulation (codenamed PEGASEMP), using doxorubicin as model payload, to be effective against solid tumors overexpressing nucleolin, as compared to long-circulating liposomes, as Caelyx [41].

Initially, design and characterization of PEGASEMP demonstrated that it was stable, presenting suitable characteristics for intravenous administration, in every other parameter comparable to Caelyx (Fig. 1), the gold standard for doxorubicin tumor delivery, based on the EPR effect [46]. In spite of zeta potential was a distinct feature under the same conditions, both PEGylated formulations presented small values in magnitude (Fig. 1f) [47]. PEGylation is known to stabilize nanoparticles through the reinforcement of repulsive hydration forces [48] and to decrease zeta potential magnitude [47,49,50]. Furthermore, PEGASEMP's size and drug retention remained stable, for at least 3 months (Fig. 1g). Together, these results indicated that zeta potential, alone, did not compromise PEGASEMP's stability, in line with the established role of PEG on colloidal stability [49]. One may speculate that the lysine-rich F3 peptide may influence PEGASEMP's zeta potential magnitude, relative to Caelyx, further contributing to the net of repulsive, inter-particulate, stabilizing forces. Notwithstanding, this has a residual influence on both cellular association, as liposomes targeted by a scrambled peptide, retaining the same amino acid composition, did not bind to nucleolin-overexpressing cancer cells (data not shown), and drug release in serum (relative to Caelyx, Fig. S1).

Facing the expected differences on pharmacokinetics between PEGASEMP and Caelyx, we questioned whether these would translate into relevant safety differences in known models used to assess Caelyx toxicology [19]. In fact, PEGASEMP was better tolerated by rats and dogs than Caelyx at the same dose, as assessed by variation of body weight or survival (Fig. 2d–f). This was likely the result of a lower systemic exposure that characterized the former (Fig. 2b, c). Impact of both PEGASEMP and Caelyx over hematological or clinical chemistry parameters was minimal, often within normal range values [20–22]. Still, there were evidences of lymphocyte depletion in rats administered with PEGASEMP (Fig. 2g, Table S1). Considering that the bone marrow is the site of origin of precursor cells

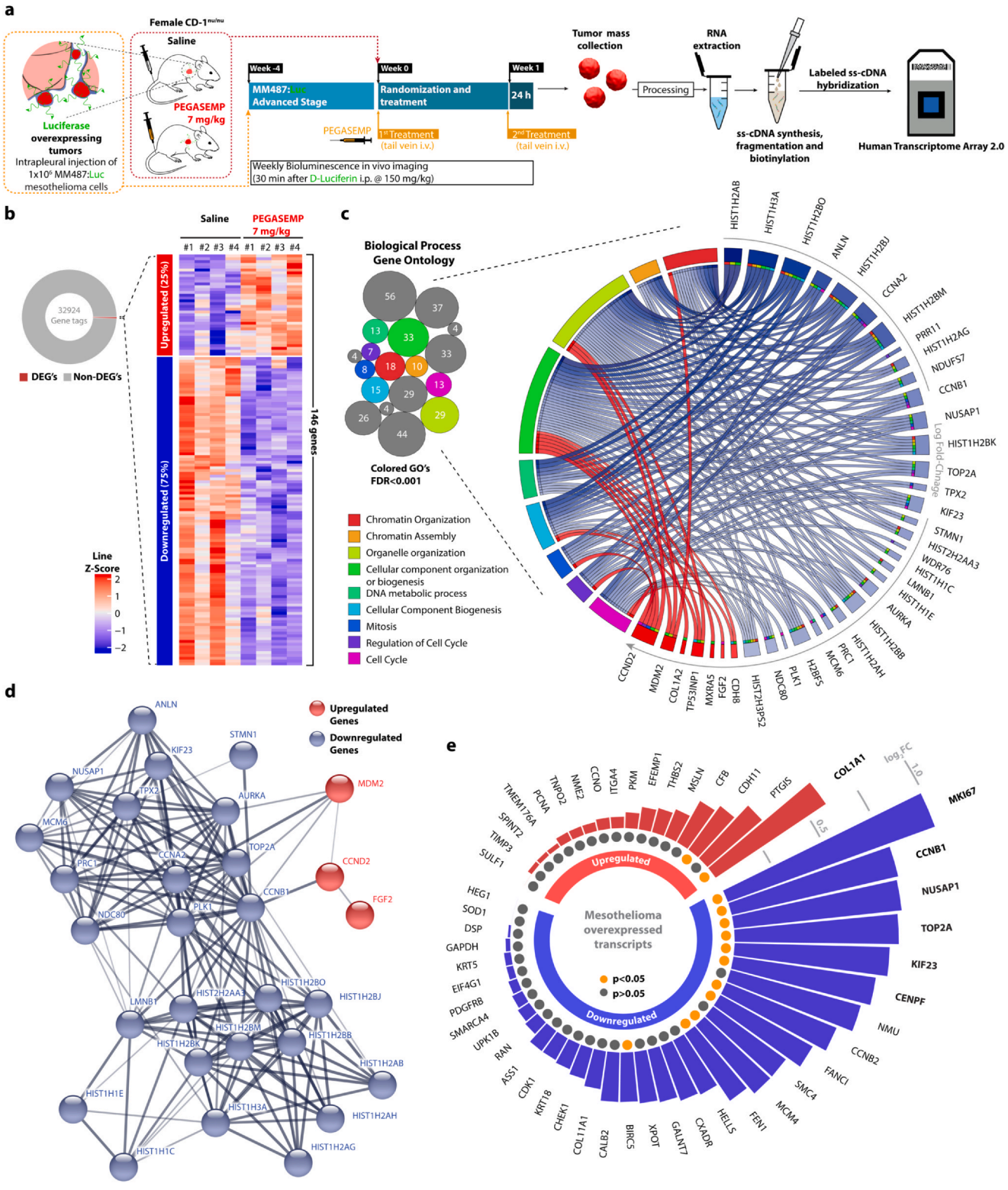

Fig. 5. Cell cycle and DNA metabolism deregulation as part of the molecular signature of PEGASEMP's in the treatment of mesothelioma. (a) Female CD-1$^{nu/nu}$ mice bearing MM487:Luc-derived tumors (at advanced stage) were treated twice, intravenously, with PEGASEMP at 7 mg/kg/week or saline as a control (n = 9/group). Twenty-four hours after the last administration, tumors were collected and processed for differential gene expression analysis between PEGASEMP-treated samples and controls using the GeneChip™ Human Transcriptome Array 2.0. (b) Heatmap of the differentially expressed genes (DEGs) among all tested gene tags. The heatmap was generated after z-score transformation of relative expression signals. (c) Gene ontology analysis (GO) of mapped DEGs against PANTHER Biological Process GO-Slim database. Bubble diagram represents the number of altered transcripts per GO's. The chord diagram represents the mapped DEGs against the top Biological Process-associated GOs (FDR < 0.001). Genes are ordered by increasing fold-change (log_2) (Blue gradient – downregulated genes; red gradient – upregulated genes). Ribbon thickness encodes the absolute logFC value for each gene. (d) STRING analysis of the functional interaction between DEGs represented in (c). Each node represents a gene/protein. Line thickness and color intensity encode confidence on protein-protein interaction. Nodes with unknown interaction were omitted. (e) Impact of PEGASEMP on malignant mesothelioma-associated overexpressed transcripts (gene list was described by Barone et al. [32]). Data represent the mean fold-change (log_2FC) relative to saline (difference p-value is indicated by – yellow/black colored circles, n = 4). Highlighted genes (bold) fit the differential expression criteria (p-value < 0.05 and absolute log_2FC > 0.58). (For interpretation of the references to color in this figure legend, the reader is referred to the web version of this article.)

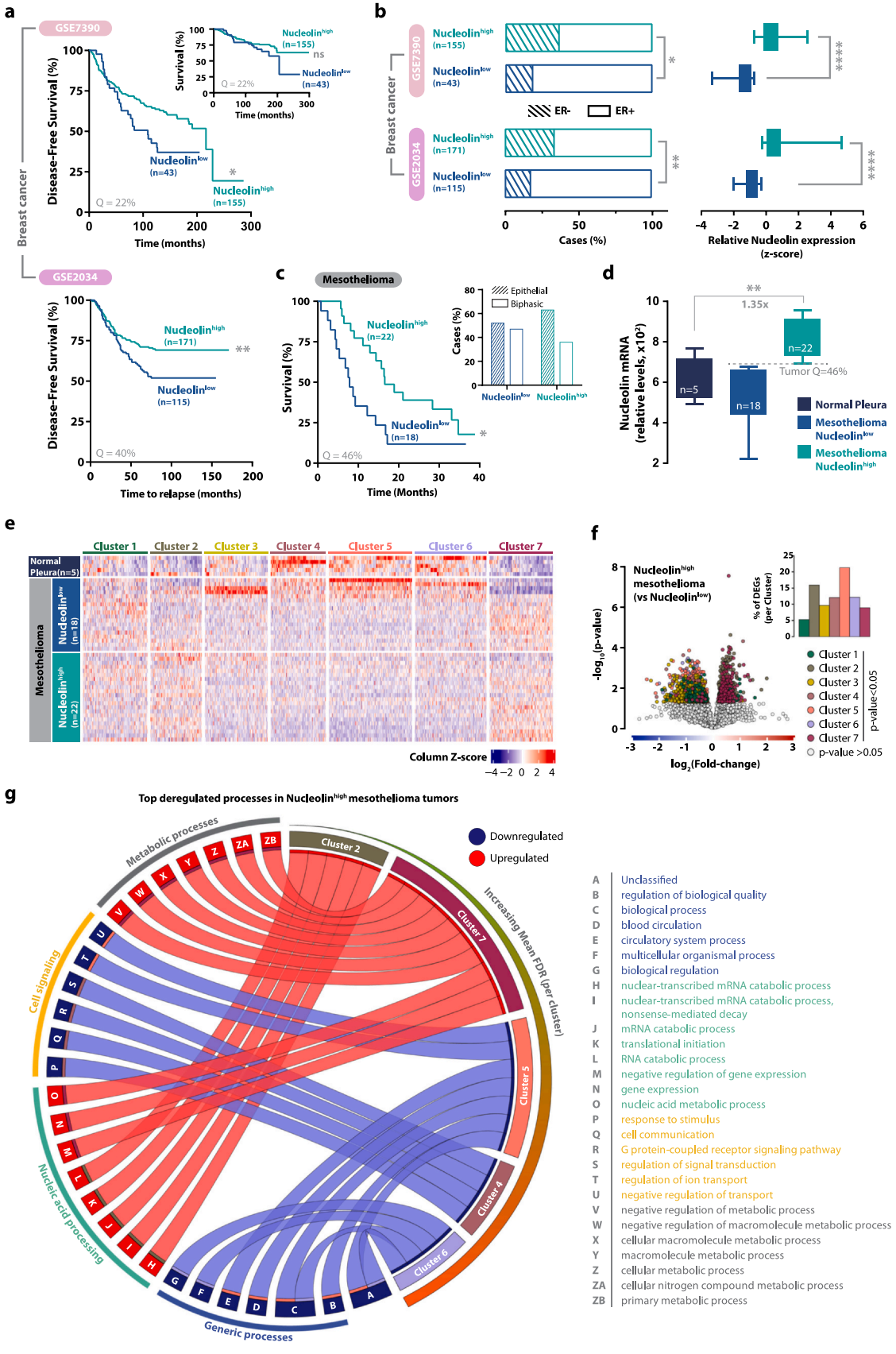

(caption on next page)

Fig. 6. Nucleolin expression in primary human breast and mesothelioma tumors. (a) Time-to-event analysis of two independent breast cancer datasets (GSE7390 and GSE2034 [n = 198 and 286 patients, respectively]) according to nucleolin mRNA levels (nucleolin^{low} and nucleolin^{high}) in primary tumors, stratified at identified quantiles (Q) (p-values calculated by logrank Mantle-Cox test). (b) Distribution of estrogen receptor (ER) status across breast tumors (p-value calculated with χ^2 test) according to relative nucleolin mRNA levels (p-value calculated with Mann-Whitney test). (c) Survival data analysis of mesothelioma patients (GSE2549 dataset, n = 45) based on nucleolin mRNA levels in primary tumors (insert: mesothelioma subtype distribution across nucleolin^{low} and nucleolin^{high} tumors) (p-values calculated by logrank Mantle-Cox test). (d) Nucleolin expression in primary human mesothelioma tumors relative to normal pleura tissue (p-value calculated with Dunn's test). (e) Mesothelioma microarray (22283 genes) heatmap of clustered genes (z-score-based k-means) upon tumor stratification using survival's optimum cutoff (Q = 46%), and compared to normal pleura tissue. (f) Volcano-plot of cluster-specific differentially expressed genes (DEGs) (p-value < 0.05, calculated using *t*-test) between nucleolin^{low} and nucleolin^{high} mesothelioma tumors (insert: distribution of DEGs across clusters). (g) Chord plot of the top deregulated processes (lowest false discovery rate, FDR) *per* cluster, upon mesothelioma's DEGs mapping against PANTHER Biological Process database (number of ontologies *per* cluster reflects the relative percentage of each cluster contribution for the total mapped ontologies). $^{ns}p > 0.05$, $^{*}p < 0.05$, $^{**}p < 0.01$, $^{****}p < 0.0001$.

originating B-cell and T-cell progenitors in the peripheral lymphoid tissues, the bone marrow aplasia arising from PEGASEMP administration was considered the main cause of the lymphocyte depletion, further observed in the thymus, spleen and lymph nodes [51], but still in an extent lower than Caelyx (Fig. 2h). This is compatible with the toxicity profile described for anthracyclines, which includes hematopoietic suppression, often associated with increased oxidative stress through induction of free radical production [52]. Nevertheless, lymphocyte depletion is a common non-specific change related to stress [51], and therefore contribution from stressful conditions cannot be ruled out from the lymphoid changes. Anthracyclines are also associated with dose-limiting cardiotoxicity [53]. However, cardiac function-related changes (Troponin I (Fig. 2g, Table S4)) upon PEGASEMP administration were transient and recoverable, not presenting any evidence of histological lesion. Thus, the residual impact of PEGASEMP over cardiac function is consistent with the protection originally provided by a liposomal formulation [41]. Mainly in dog males, testes were significantly affected by PEGASEMP treatment (Fig. S3b), related with anthracycline action. Nevertheless, the presence of normal Sertoli cells, accompanied by formation of a meshwork around developing germ cells [54], suggested organ recovery.

Having PEGASEMP presented an overall more favorable toxicological profile than Caelyx, at the cost of a lower systemic exposure (Fig. 3b), it was surprising that PEGASEMP enabled the same impact on tumor burden as Caelyx, against nucleolin^{high} tumors (Fig. 3b). This result would have not been possible if the antitumor effect of PEGASEMP solely relied on an EPR-based tumor accumulation. Herein, a number of aspects have been identified that could support these results.

The assessment of doxorubicin in the tumor by two different techniques, not often seen in the literature, as liquid-chromatography-tandem mass spectrometry (indicative of drug bulk accumulation in the tumor) and confocal microscopy (indicative of doxorubicin^{+} tumor cells), was crucial to better understand the mechanism of action of PEGASEMP relative to Caelyx. In fact, the similar tumor delivery index provided by the former methodology (Fig. 3b) was not predictive of the higher tumor bioavailability index of PEGASEMP relative to Caelyx, as demonstrated by the latter technique (Fig. 3b, d) [55]. This was not the case of liposomes functionalized with a monoclonal antibody targeting the HER2 antigen, overexpressed in (poorly accessible) cancer cells, and thus highly dependent on the EPR effect to reach the target. In fact, this targeted formulation presented the same extent of accumulation in breast tumors as the non-targeted counterpart, besides a similar systemic exposure [56]. Interestingly, the advantage of PEGASEMP on tumor burden, over non-treated mice, was actually dissipated upon assessing activity against tumors derived from nucleolin^{low} 4T1 cells, yet more sensitive to PEGASEMP than nucleolin^{high} MDA-MB-435S *in vitro* (Fig. S6). In addition, at the tumor level, PEGASEMP markedly decreased by 19-fold the nucleolin^{+} vasculature relative to Caelyx (Fig. 3b, c), an observation aligned with the N6L peptide-mediated targeting of nucleolin^{+} tumor angiogenic blood vessels [14,57].

The previous results supported an association between the anticancer activity of PEGASEMP and nucleolin tumor expression. This was further reinforced by the combined demonstration of the specific nucleolin clustering into membrane raft-like domains triggered by F3 peptide (in the form of DSPE-PEG_{2k}-F3 micelles), in line with other several specific (nucleolin-binding) ligands (as midkine, pleiotrophin or HB-19) [58–60], and the further inhibition of cellular association of F3 peptide-targeted liposomes upon blocking N-glycosylation (impairing nucleolin translocation to the cell surface [31]).

Under the EPR paradigm [61], the antitumor effect of PEGASMEP against nucleolin^{high} expressing tumors (Fig. 3d, e), subsequent to the enhanced intracellular delivery and improved intratumor bioavailability of doxorubicin (Fig. 3b, d), could be hardly anticipated given the lower systemic exposure of doxorubicin (assessed by mass spectrometry (Fig. 3b)), relative to liposomes devoided of ligand-mediated targeting and trigger release components. One might argue that the enhanced bioavailability of doxorubicin provided by PEGASEMP (Fig. 3b) should translate to superior antitumor effect compared to Caelyx. Yet, the administration frequency to determine each parameter was distinct, and multi administration could actually compromise over time the nucleolin positive tumor vasculature and, subsequently, the tumor delivery and bioavailability indexes of PEGASEMP (as well as Caelyx), which remains to be fully determined. Nonetheless, collectively, the results supported a nucleolin-dependent drug delivery mechanism into nucleolin^{high} solid tumor, lessening the dependence on both elevated systemic exposures (and associated side effects) and the EPR effect (Fig. S7), demonstrated to take place in limited extent in patients, which has been compromising efficacy [61].

The therapeutic efficacy and safe toxicological profile of PEGASEMP, underlying the mechanism of drug delivery associated with pH-sensitive pegylated liposomes targeted to nucleolin, and the given mechanism of action of its payload, urged us to test PEGASEMP's therapeutic relevance in an highly invasive and proliferative disease, as pleural mesothelioma [33]. As it overexpressed nucleolin, (Fig. 4a), PEGASEMP was highly effective in controlling epithelioid mesothelioma tumor growth, in monotherapy, as compared to the standard of care (Fig. 4c, d), an observation of utmost importance given the fact that the model was derived from cells of a patient in disease progression, previously treated with the standard of care (pemetrexed + cisplatin) [62]. Hence, this animal model was resistant to pemetrexed and partly to cisplatin, thus recapitulating a highly relevant clinical situation [63]. Furthermore, the antitumor effect of a water-soluble anti-nucleolin aptamer-paclitaxel conjugate (NucA-PTX) was recently characterized against ovarian tumors [64]. NucA-PTX enabled a 33% reduction of tumor growth at the end of experiment, as compared to the non-specific counterpart or free drug (standard of care) [64]. Notwithstanding the antitumor effect was not as extensive as PEGASEMP's, attributable to differences associated with the nature of the delivery system as well as tumor model, both results reflect the importance of nucleolin as a target for enhanced drug delivery.

Additionally, the therapeutic impact of PEGASEMP, alone or combined with cisplatin, over tumor invasion of chest cavity (Fig. 4j) provided support for a neoadjuvant regimen against mesothelioma [65]. Furthermore, the results obtained with PEGASEMP as single treatment in the biphasic models suggested that disease stage may

influence the therapeutic outcome, as often described in the clinic [66]. Early-treated (epithelioid and biphasic) tumors may be responsive to PEGASEMP in monotherapy, while advanced biphasic mesothelioma may benefit from a combination of PEGASEMP and cisplatin (Fig. 4d, i). Molecularly, the antitumor effect of PEGASEMP against mesothelioma relies on a deregulation of cell division through downregulation of cell cycle and DNA metabolism-related processes, as indicated by comparative transcriptomic analysis (Fig. 5), including the downregulation of transcripts consensually described as overexpressed in malignant mesothelioma (Fig. 5e) [32] and strongly involved in cell division processes, such as topoisomerase 2, cyclin B1 or the proliferation marker Ki67 (TOP2A, CCNB1 or MKI67, respectively) (Tables S8, S9). Furthermore, while p53 upregulation was not observed (Fig. S9 and Table S8), upregulation of MDM2 and TP53INPI (Fig. 5c) could be associated with doxorubicin-mediated oxidative stress [53]. Alternatively, upregulation of COL1A2 and FGF2 may be the result of a fibrotic process associated with the treatment, and predictive of longer overall survival and disease-free survival [67]. Thus, PEGASEMP affected, in part, the molecular signature of malignant mesothelioma by impairing cell division, consistent with the mechanism of action of doxorubicin [53]. In fact, the querying of breast and mesothelioma datasets demonstrated a direct correlation between high nucleolin mRNA levels and better patient prognosis, compared to low-expression cancers (Fig. 6a, c) and in accordance with previous observations [37]. Furthermore, it was observed a higher frequency of ER- tumors in nucleolin^{high} breast cancer groups and a biological distinction of nucleolin^{high} mesotheliomas from those nucleolin^{low}, favoring nucleic acid metabolism on the former (Fig. 6b, g). Altogether, and in the context of PEGASEMP's preclinical efficacy and safety data above (Figs. 2–4), those observations suggested that nucleolin-targeting strategies may be potentially effective alternatives in the treatment of patients with nucleolin-overexpressing tumors that may lack the therapeutic options or the effectiveness from the standard of care, as ER- breast cancer and mesotheliomas, respectively.

Conclusions

The difficulties in treating solid tumors, are transversal to a number of different strategies targeting overexpressed markers, as anticancer nanomedicines or antibody drug conjugates, aiming at acting locally while avoiding systemic activity, and thus improve anticancer efficacy and reduce toxicity to healthy tissues. In the case of anticancer nanomedicines, the reduced percentage of injected dose (lower than 1%, Ref. 9) that reaches the tumor, along with the limited access to the tumor microenvironment, illustrated by EPR-based nanomedicines like Caelyx, have represented barriers themselves. They limit the accomplishment of the full potential of nanomedicines in the treatment of solid tumors. It is thus important to engineer novel delivery mechanisms that make the best use of the limited dose reaching a solid tumor. To address these challenges, pH-sensitive pegylated liposomes, based on unsaturated phosphatidylethanolamines, as DOPE, and mildly acidic amphiphiles that act as stabilizers at neutral pH, as CHEMS, have been combined with a component of nucleolin targeting (PEGASEMP). In other words, the efficient intracellular pH-triggered release and rapid blood clearance of the former have been combined a targeting component towards a marker readily accessible in the tumor vasculature, besides cancer cells. The results herein presented support a novel mechanism of drug delivery towards nucleolin-overexpressing solid tumors. It lessens the dependence on the EPR effect in respect to the antitumor activity, while maintaining a safer toxicological profile, arising from a lower systemic exposure, relative to the gold standard delivery system for doxorubicin, Caelyx. Notwithstanding the thorough toxicokinetic assessment performed in three different species, including mice, rats and dogs, efficacy needs to be further complemented with immunocompetent animal models. Nevertheless, the approval of the anti-PD-L1 monoclonal antibody Atezolimumab combined with the paclitaxel-containing nanoparticles (Nab-paclitaxel) [68] is a good example on how a nanoparticle and its encapsulated payload can synergize with the immune tumor microenvironment. In fact, the former is described to enhance the priming and lytic activity of $CD8^+$T cells [69]. A payload like doxorubicin could increase the immunogenicity of malignant cells by inducing immunogenic cell death, resulting in stimulation of myeloid cells to differentiate into antigen-presenting cells and thus triggering effective adaptive immune responses [70].

Overall, the work herein presented support nucleolin as a cornerstone target to be exploited in a clinical setting, against nucleolin-overexpressing tumors of diverse histological origin. Furthermore, the demonstration that PEGASEMP targeting effectiveness depends on nucleolin overexpression, as expected, anticipates the need of an adequate patient stratification to ensure adequate outcome predictability. Collectively, the pharmacodynamic insight on PEGASEMP that underlies its antitumor effect across different tumor models, reflected its potential as a novel nanomedicine, with the ability to introduce a significant benefit in terms of efficacy against nucleolin-overexpressing human tumors, as well as in terms of safety.

Materials and methods

Liposomes

A 3 L pilot batch of PEGASEMP (and an empty version) was produced by ethanol injection method at Evonik Canada (former Northern Lipids, Canada) under *Good Manufacturing Practices* conditions. Resulting multilamellar vesicles were extruded through 80 nm membranes to form large unilamellar vesicles. Encapsulation of doxorubicin was performed through remote loading [71]. Sterile filtration was performed before vial filling. Assessment of residual solvents (result: not detected), bacterial endotoxins (result: < 0.8 EU/mL) and sterility (result: no growth) was validated according to USP (United States Pharmacopeia) < 467 >, USP < 85 > and USP < 71 > monographs, respectively. Alternatively, liposomes with a similar lipid composition of PEGASEMP were fluorescently labeled upon incorporating 1 mol% of Rhodamine-PE in the formulation, and further prepared by ethanol injection method [72].

Cell culture

Nucleolin-overexpressing MDA-MB-435S cell line and 4T1 murine triple-negative breast cancer cells were acquired from ATCC (Virginia, USA) and cultured in RPMI 1640 (Sigma-Aldrich, USA) supplemented with 10% (vol/vol) of heat-inactivated Fetal Bovine Serum (FBS) (Invitrogen, USA), 100 U/mL penicillin, 100 µg/mL streptomycin (Lonza, CH) and maintained at 37 °C in a 5% CO_2 atmosphere. The pemetrexed and cisplatin resistant epithelioid MM473 and the biphasic MM487 mesothelioma lines were isolated from patients as previously described [62]. Both cell lines were cultured in Ham's F-10 Nutrient Mixture medium (Gibco, USA) supplemented with 10% (vol/vol) of heat-inactivated FBS (Gibco, USA) and 0.05 mg/mL of gentamicin sulfate (EuroClone, IT) and maintained at 37 °C in a 5% CO_2 atmosphere. From those, luciferase-expressing MM473:Luc and MM487:Luc were obtained as described [63]. For *in vivo* studies, MM473:Luc and MM487:Luc were cultured in Ham's F-10 Nutrient Mixture medium, supplemented with 10% (vol/vol) FBS and 400 µg/mL of neomycin, and expanded in a 37 °C incubator with saturated humidity and 5% CO_2. Cells were routinely tested for mycoplasma contamination, using MycoAlert Mycoplasma Detection kit (Lonza, CH). Cells were authenticated by examination of morphology and consistent *in vitro* performance.

Animals and animal models

Female BALB/c mice [BALB/cAnNCrl], BALB/c nude mice [CAnN.Cg-Foxn1^{nu}/Crl] and female CD-1 nude mice [Crl:CD1-Foxn1^{nu}] (Charles River, FR or IT), were housed in individually ventilated cages on a 12 h light:12 h dark cycle at 20–24 °C and 45–65% humidity. Mice were allowed free access to sterilized diet and water. To generate a model of nucleolin-overexpressing tumor, 2.5×10^5 MDA-MB-435S cells were orthotopically injected in the mammary fat pad of 5-week-old female BALB/c nude mice. The low nucleolin-expressing tumors were generated upon the orthotopic injection of 500 triple-negative 4T1 murine breast cancer cells into the mammary fat pad of 5-week-old female BALB/c mice. Tumors were measured twice a week with a caliper and tumor volume (TV) was determined using the equation $TV = 0.5 \times L \times W^2$, where *L* is the length of longest axis and *W* is the length of shorter axis. Human mesothelioma mouse models were generated as previously described [63]. Briefly, 1×10^6 mesothelioma cells were orthotopically injected intrapleurally (i.pl.) in 4–5 weeks-old female CD-1 nude mice, under deep isoflurane anesthesia. Cell engraftment was followed for until treatment start (described below) through the IVIS Spectrum (PerkinElmer, USA) *in vivo* imaging technology, for the evaluation of the bioluminescence signal radiance (p/s/cm^2/sr), 30 min after i.p. administration of D-Luciferin (150 mg/kg). Once tumors reached adequate size, animals were randomly allocated to treatment groups.

Experiments with rats and beagle dogs were performed at Aptuit (Verona, IT), an Evotec Company, under *Good Laboratory Practices (GLP)* guidelines. Nine weeks-old female and male CD® IGS rats [Crl:CD(SD)] (Charles River, IT) were housed under a 12 h light:12 h dark cycle at 20–22 °C and 45–65% humidity. Rat maintenance diet Altromin R and filtered water was available *ad libitum*. Nine-months-old female and male beagle dogs (Marshall, Bioresources, FR) were housed in concrete/solid-floor pens with sawdust litter under a 12 h light:12 h dark cycle at 19–21 °C and 45–65% humidity. To each dog, a daily portion of 350 g of pelleted diet (Harlan Teklad 2021) was provided. On administration days, food was provided approximately one hour after dosing. Food was available to animals overnight but was withdrawn early in the morning. Filtered water was freely available.

Live cell confocal microscopy evaluation of cell surface nucleolin

Forty thousand MDA-MB-435S cells were seeded in 8-well microscopy µ-slide (Ibidi, DE). Twenty-four hours later, the cells were pre-incubated at 4 °C for 1 h followed by 5 min of cold PBS-BSA. Cells were then incubated 15 min at 4 °C with PBS-BSA containing 16.7 µM of PE-PEG$_{2k}$-F3 micelles and 10 µg/mL anti-NCL-Alexa®488 antibody [mouse 364-5 clone] (Abcam, UK) or the respective IgG1$_k$ isotype (Affymetrix, USA). Cells were then washed 2x with PBS-BSA and incubated with Hoechst for 10 min at room temperature. Hoechst excess was removed by 3x wash with PBS. Cell were maintained in 200 µL of PBS, and image acquisition (1508 × 1508 pixels) was performed using the LSM 710 AxioObserver confocal microscope, equipped with a Plan-Apochromat 63x/1.4 Oil DIX M27 objective, controlled by Zen 2012 SP1 v8.1.3.484 (64-bit) software (Zeiss, DE).

Nucleolin protein levels upon incubation with micelles functionalized with the F3 peptide

Nucleolin protein levels were assessed by western blot upon incubation with DSPE-PEG$_{2k}$-F3 micelles. Eight hundred thousand cells of each cell line were left undisturbed for 30 min and then centrifuged for 3 min at 170g; cell pellets were resuspended in 10 mM phosphate buffered saline (138 mM NaCl and 2.7 mM KCl) containing 1% bovine serum albumin (wt/vol) and incubated for 20 min. Cells were further centrifuged for 3 min at 170g, resuspended in PBS-BSA either alone or containing 16.7 µM PE-PEG$_{2k}$-F3 micelles and incubated for 60 min, at 37 °C. Cells were then washed twice with cold PBS and harvested and sonicated in RIPA buffer (50 mM Tris, pH 8.0, 150 mM NaCl, 1% NP-40, 0.1% SDS, 0.5% sodium deoxycholate, 1 mM EDTA, 1 mM EGTA, 1 mM DTT, 1 mM PMSF, and a cocktail protease inhibitors and phosphatase inhibitors). Equal amounts of protein (10 µg) were resolved on 10% sodium dodecyl sulfate (SDS) polyacrylamide gels and transferred onto poly(vinylidene difluoride) (PVDF) membranes. Immunoblotting was performed using the anti-NCL antibody (mouse monoclonal EPR7952, 3.4 ng/mL, Abcam, UK) and the anti-GAPDH (mouse monoclonal GA1R, 0.5 µg/mL, ThermoFisher, USA) as loading control, and revealed by chemifluorescent reagent (Amersham, USA). Semi-quantitative analysis was carried out using ImageLab 4.1 image analysis software.

Impact of F3 peptide on surface levels of other cell surface proteins

Two hundred and fifty thousand MDA-MB-435s cells were incubated with 10 µg/mL anti-NCL-Alexa®488 antibody [mouse, 364-5 clone] (Abcam, UK), 0.6 µg/mL anti-NP1-PerCP-eFluor710 [mouse, TNKUSOHA clone] (Invitrogen, USA) and 0.5 µg/mL anti-CD44-PECy5 [rat, IM7 clone] (Abcam, UK) for 1 h at 37 °C in the presence or absence of 16.7 µM PE-PEG$_{2k}$-F3 micelles, in PBS with 1% BSA. As controls, the respective IgG isotypes were used at the same concentrations. Cells were then washed twice with PBS and stained with LIVE/DEAD Fixable Far Red reagent (Life Technologies, USA), as per manufacturer instructions, to exclude death cells and immediately analyzed in a FACScalibur flow cytometer (BD Biosciences, US). A total of 20,000 events were collected and analyzed.

Cellular association of fluorescently labeled F3 peptide-targeted liposomes

Two hundred and fifty thousand MDA-MB-435s cells were incubated in presence or absence of 5 µg/mL tunicamycin (Sigma-Aldrich, USA) for 24 h at 37 °C. Cells then incubated with 0.4 mM of F3 peptide-targeted liposomes fluorescently labeled with rhodamine, for 1 h at 37 °C. Non-targeted liposomes were used as controls. Cells were then washed with PBS (3 times) and immediately analyzed in a FACScalibur flow cytometer (BD Biosciences, US). A total of 20,000 events were collected and analyzed.

Antitumor activity of PEGASEMP against murine models of cancer

The antitumor activity of PEGASEMP was evaluated against breast tumors. Animals bearing nucleolin-overexpressing MDA-MB-435S-derived tumors (100–150 mm^3) were treated with PEGASEMP at 7 mg of doxorubicin/kg, once a week, for 5 weeks. Additionally, as controls, animals were treated with Caelyx at 5 mg/kg or the saline solution, once a week, for 5 weeks. Alternatively, animals bearing 4T1 triple-negative breast tumors (50–90 mm^3) were treated with 7 or 9 mg of doxorubicin/kg, once a week, for 5 consecutive weeks. Animals treated with saline solution were used as controls. On both models, tumor volume was monitored twice a week, as well as body weight, signs of stress, and general wellbeing. Animals were euthanized one week after 5th treatment. Humane endpoints including body weight below 90% (of initial weight, Week 0) or a tumor volume above 700 mm^3 lead to early animal termination. Signs of specific secondary side effects of liposomal doxorubicin and movement impairment (owed to tumor growth) were also accounted. Upon euthanasia, tumors were collected, fixed in Tissue-Tek Xpress® Molecular Fixative (Sakura, USA), and embedded in paraffin until use.

Additional antitumor activity of PEGASEMP was determined in orthotopic mouse models of mesothelioma. Two weeks (MM473:Luc), 3 weeks (MM487:Luc Early Stage) and 4 weeks (MM487:Luc Advanced Stage) after cell injection, animals were randomly allocated to different treatment groups: saline; PEGASEMP at 5.6 or 7 mg of doxorubicin/kg; cisplatin at 4.0 mg/kg alone or combined with PEGASEMP at 5.6 mg of

doxorubicin/kg, weekly administered for 5 weeks (q7dx5). A control group was administered with the standard of care (a combination of cisplatin at 4.0 mg/kg (q7dx5) plus pemetrexed at 100.0 mg/kg, thrice a week, for 5 weeks (q2dx3×5)) [25,73]. Cisplatin posology and schedule matched its MTD as a single agent, in mice [74]. Bioluminescence, as a measure of tumor growth, was monitored weekly as above. Body weight was recorded weekly to evaluate potential toxic effects of the treatments. At experiments end, mice were euthanized and submitted to complete necroscopy. Thereafter, the parietal and visceral pleura and the respective organs of all the animals were preserved in a 10% buffered formalin solution, until use.

Nucleolin and CD31 area staining determination using StereoInvestigator-based approach

The area occupied by nucleolin and CD31-positive cells was determined in MDA-MB-435S-derived tumors randomly selected from the subset of animals that underwent 5 treatments in each group. Briefly, 4 tumors sections/tumor (n = 3–4 tumors *per* group) were processed using IHC procedures as described above. Each slide was then analyzed in an AxioImager Z2 microscope using a Plan-Apochromat 40x/1.3 Oil objective (Zeiss, DE), controlled by StereoInvestigator v11.03.1 software (MBF Bioscience, USA). For every section, the tumor area was digitally defined. StereoInvestigator was then configured to place a 200 × 200 µm counting frame every 800 µm in a grid automatically and randomly established within the defined tumor area. The corresponding sampling area was then swept using the area fractionator tool and the area (in percentage) occupied by the cells of interest, within the sampling area, was established.

Pharmacokinetics of doxorubicin-containing PEGASEMP

Doxorubicin blood clearance profile was evaluated in both female BALB/c and female MDA-MB-435S tumor-bearing BALB/c nude mice (once tumors have reached 100–150 mm^3). Briefly, animals were randomly allocated to different groups according to formulation or administered dose (n = 15–16 animals *per* group). PEGASEMP was intravenously administered, in the tail vein, at 5, 6 and 7 mg of doxorubicin *per* kg of body weight. As a control, non-targeted non-pH sensitive liposomal doxorubicin (Caelyx) was administered by the same route, 5 mg of doxorubicin/kg. Within each group, mice were divided into four subsets (n = 3–4 animals *per* subset) according to the timepoint of blood collection (2 bleeds *per* animal). The tubes (K_3EDTA-coated) were centrifuged at 800*g* for 10 min, at room temperature, and plasma was collected and stored at − 80 °C until analysis. When appropriate, animals were euthanized, and MDA-MB-435S-derived tumors were collected, snap-frozen in liquid nitrogen and stored at − 80 °C, until further analysis.

In another set of pharmacokinetics studies, PEGASEMP was intravenously administered at 1 or 2 mg of doxorubicin/kg to male and female beagle dogs (n = 3 *per* sex gender) or male and female CD® IGS rats (n = 3 *per* sex gender), once every week for 4 consecutive weeks. Control groups, consisted of Caelyx at 1 or 2 mg of doxorubicin/kg, in the dog or rat experiments, respectively. Further control in both species included the administration of saline vehicle solution of PEGASEMP. The blood clearance profile of doxorubicin was established following first intravenous administration of PEGASEMP. Serial blood collection (0.5, 1, 2, 5, 8, 24 and 48 h after administration) was performed into K_3EDTA-coated tubes. Upon centrifugation, plasma was collected and stored at − 20 °C until analysis.

Intratumoral localization of doxorubicin by laser confocal microscopy

Previously frozen MDA-MB-435S-derived breast tumors (approximately 150 mm^3, 4 tumors *per* group), recovered 24 h after single i.v. administration of PEGASEMP at 6 and 7 mg of doxorubicin/kg or Caelyx at 5 mg of doxorubicin/kg, were thawed, sliced in half, and mounted onto disposable base molds. The tumor tissues were immediately embedded in OCT compound (Tissue-Tek Sakura, NL) and stored at − 80 °C. Thirty microns sections were obtained in a CM3050S Cryostat (Leica, DE) using DB80LS blades (Leica, DE). Two random cuts (each with two tumor sections, one from each half) were placed on SuperFrost® Plus slides (ThermoFisher, USA), washed with phosphate buffer saline, PBS (1.4 mM potassium phosphate monobasic, 2.7 mM potassium chloride, 4.3 mM disodium hydrogen phosphate and 137 mM sodium chloride, pH 7.4), and mounted using Fluoroshield® mounting medium with DAPI (Abcam, UK), and allowed to dry at room temperature in the dark. Two slides from each tumor were collected (8 slices *per* tumor).

Each tumor slice area was fully inspected for doxorubicin fluorescence using LSM 710 AxioObserver confocal microscope using Plan-Apochromat 40x/1.4 Oil objective controlled by Zen 2012 SP1 v8.1.3.484 (64-bit) software (Zeiss, DE). Area swept and image acquisition (1024 × 1024 pixels/0.045 mm^2) were performed blindly by the operators to minimize bias. Image analysis was performed blindly using Zen v2.0 software (blue edition, 64-bit, Zeiss, DE) enabling one to count doxorubicin positive cells.

Gross pathology, histopathologic analysis and scoring of mesothelioma-derived lesions

On necropsy, animals bearing MM437:Luc-derived mesothelioma tumors were inspected for evidences of grossly detectable chest invasion, pleural/visceral plaques and microscopic evidence for pulmonary lesions. On a qualitative basis and depending on the extent of the lesion of the area of the affected lobe, pulmonary lesions were grouped as follows: from small to medium-sized, large-sized or massive for lesion extent lower than 10%, ranging from 10% to 20%, or higher than 20% up to 50%, respectively. Accordingly, the combined information on the neoplastic lesions were scored as follows: (a) *slight* – for variably-sized pleural plaque/s only; (b) *mild* - variably-sized pleural plaque/s only, in presence of large visceral plaques; (c) *moderate* - small to medium-sized pulmonary infiltrate, possibly in presence of variably-sized pleural plaques; (d) *severe* - variably-sized pulmonary infiltrates/large-sized pulmonary infiltrate, possibly in the presence of variably-sized pleural plaques; and (e) *marked* - massive pulmonary infiltrate, possibly in the presence of variably-sized pleural plaques. The percentage of animals falling within a category range was determined and plotted for each treatment group.

Differential gene expression in mesothelioma upon PEGASEMP treatment

Female CD-1 nude mice bearing the MM487:Luc advanced biphasic mesothelioma tumors (see above), were treated twice, intravenously, with PEGASEMP at 7 mg/kg/week (n = 9/group). Saline was used as control following the same schedule. This schedule enabled the collection of tumor masses with enough material for analysis, otherwise unviable with longer treatments. Twenty-four hours after the last treatment, tumor masses were collected and snap-frozen in liquid nitrogen and stored at − 80 °C. Upon RNA extraction (TriFast Gold Reagent [Euroclone, IT] in combination with TissueLyzer (Qiagen, USA) programmed for 20 Hz for 3 min), four randomly select samples from each group were subjected to retro-transcription, labeling and hybridization using HTA2.0 Plus Reagents KIT (Affymetrix, USA). Samples were profiled using the GeneChip™ Human Transcriptome Array 2.0 (HTA2.0, Affymetrix, USA). Processing and downstream analysis of the experimental data was performed with R (version 3.5.0), using *Bioconductor Oligo* package (version 1.44.0) [75] for the oligonucleotide microarray-preprocessing with the RMA algorithm [76,77], which includes background

subtraction, normalization and summarization steps. Identification of the differentially expressed genes (DEGs) for PEGASEMP-treated tumors was performed relative to non-treated tumors, using *limma* package (version 3.36.1) [78]. The data have been deposited in NCBI's Gene Expression Omnibus [79] and are accessible through GEO Series accession number GSE121205 (https://www.ncbi.nlm.nih.gov/geo/query/acc.cgi?acc=GSE121205). DEG's were determined considering the cutoff values of difference p-value < 0.05 and absolute $\log_2$FC > 0.58. Gene ontology (GO) annotation of DEG's was performed using the PANTHER-powered Gene Ontology Consortium database (geneontology.org) using PANTHER GO-Slim Biological and Cellular component datasets (version 13.1). STRING analysis (string-db.org, version 10.5) was also performed to predict functional interaction between DEG's, highlighting functional enrichments. Furthermore, data visualization was designed using RStudio (v1.1.453) with relevant R packages [*ggplot2* (v3.0.0) and *ComplexHeatmap* package (v1.18) [80] after z-score [$z = (x-\mu)/\sigma$] transformation of relative expression signals], and Circos Online tool [81].

Assessment of PEGASEMP impact on hematological and clinical chemistry parameters of rats and dogs

At week 3 and 4, blood was collected from dogs and rats, respectively (either administered with PEGASEMP or controls), into tubes containing K_3EDTA. Hematological parameters (red blood cells [and respective size distribution], reticulocytes, white blood cells [with differential analysis of neutrophils, lymphocytes, monocytes, eosinophils, basophils] and platelet counting, and further evaluation of hemoglobin, hematocrit, mean cell volume, mean cell hemoglobin and mean cell hemoglobin concentration) were assessed in an ADVIA® 120 automated hematology system (Siemens, DE). At the same timepoints, blood was collected into serum collection tubes without anticoagulant for analysis of clinical chemistry parameters. Serum enzyme levels (Alkaline Phosphatase, Alanine Aminotransferase, Aspartate Aminotransferase, Glutamate dehydrogenase, Creatine Kinase), total bilirubin, creatinine, protein content (total protein and albumin), inorganic content (potassium, sodium, calcium, chloride, inorganic phosphorus), lipid (triglycerides and cholesterol) and glucose levels were determined using an ADVIA® 1650 automated clinical chemistry system (Siemens, DE). Normal reference intervals for rats and dogs at similar age were collected from literature [20,21] and Charles River reference values [tinyurl.com/y7s4o8rh].

Evaluation of treatment-associated cardiotoxicity in beagle dogs

Assessment of the plasma levels of cardiact troponin I (cTnI) was performed in beagle dogs as a measure of the potential direct cardiac toxicity of PEGASEMP. Briefly, blood plasma was collected into tubes without anticoagulant, 2 weeks after treatment initiation from the animals involved in the toxicokinetic study. Plasma levels of cTnI were then determined using a highly sensitive chemiluminescence method (Acridinium Ester TnI-Ultra assay, Siemens, DE) on ADVIA Centaur® CP Immunoassay high-throughput bench top system (Siemens, DE). Normal reference intervals at similar age were collected from literature [22].

Patient survival and data analysis

GEO datasets from breast cancer (GSE7390 and GSE2034 [n = 198 and 286], respectively) and mesothelioma (GSE2549, n = 45) [38–40] were explored. Nucleolin mRNA expression and patient survival data were plotted considering the best cutoff provided by survminer R package (v0.4.3). Breast cancer survival analysis by subtype was not completed because the data sets are not categorized with that information. Cluster heatmap analysis was performed using k-means in R, upon data transformation to z-score. Gene ontology annotation of DEG's per cluster was performed using the PANTHER GO Biological component dataset. Data visualization was further composed as described above.

Statistical analysis

Results are expressed as mean ± SEM, unless otherwise specified. Statistical analysis (p-values, *n*'s and statistical tests) is included in the text and figure legends.

Study approval

All experiments involving mice were in accordance with the European guidelines for the care and use of laboratory animals (2010/63/EU directive) and approved by the appropriate institutional review board. The experiments with rats and beagle dogs were performed in accordance to OECD guidelines (ENV/MC/CHEM(98)17).

CRediT authorship contribution statement

N.A.F. and A.C.G. contributed equally for this work. N.A.F. and A.C.G. designed and performed experiments, analyzed data, prepared figures, wrote and edited the manuscript. V.M.M. optimized and conducted the mass spectrometry analysis. R.L. and T.A. designed experiments, performed flow cytometry, and edited the manuscript. N.G. performed western blot and contributed to data interpretation. B.M. supervised mass spectrometry experiments and analysis. M.L. and P.F. supervised breast tumors histological analysis. F.C., D.P., G.S., F.C., and C.P. designed and supervised mesothelioma experiments and edited the manuscript. L.F. designed the mesothelioma histological analysis. A.F. analyzed primary microarray data and edited the manuscript. T.C. supervised components and obtained funding for the study. L.A. contributed to the design of the rats and beagle dog experiments. M.P. provided support on patient survival analysis. M.G. provided support on the physical analysis of the liposomes. V.M. and S.S. supervised all the components of the study and edited the manuscript. J.N.M. supervised all components of this study, designed experiments, wrote and edited the manuscript.

Declaration of Competing Interest

The authors declare the following financial interests/personal relationships which may be considered as potential competing interests: V.M., N.A.F. and A.C.G. were former employees at TREAT U, SA. V.M., T.C., S.S., L.A., and J.N.M. are share-holders of TREAT U, SA. The remaining authors declare no competing interests.

Acknowledgements

We would like to thank Dr. Nuno Vilaça Marques from CHUC Pharmacy for providing Caelyx as freshly unused spares. This work was supported by the following projects: QREN/FEDER MultiNanoMed (Ref: 23240). This work was also financed by the European Regional Development Fund (ERDF), through the Centro 2020 Regional Operational Program under project CENTRO-01-0247-FEDER-017646 (ODD4PEGASEMP), and through the COMPETE 2020 - Operational Program for Competitiveness and Internationalisation and Portuguese national funds *via* FCT – Fundação para a Ciência e a Tecnologia, I.P., under projects POCI-01-0145-FEDER-016390 (CancelStem), *Euronanomed* (FCT reference ENMed/0005/2015), CENTRO-01-0145-FEDER-000012-HealthyAging2020 and CIBB (FCT reference UIDB/04539/2020) and by The National Mass Spectrometry Network (RNEM) under the contract LISBOA-01-0145-FEDER-402-022125 (POCI-01-0145-FEDER-402-022125).

Appendix A. Supporting information

Supplementary data associated with this article can be found in the online version at doi:10.1016/j.nantod.2021.101095.

References

[1] M.L. Etheridge, S.A. Campbell, A.G. Erdman, C.L. Haynes, S.M. Wolf, J. McCullough, The big picture on nanomedicine: the state of investigational and approved nanomedicine products, Nanomed. Nanotechnol. Biol. Med. 9 (2013) 1–14, https://doi.org/10.1016/j.nano.2012.05.013

[2] M.E. O'Brien, N. Wigler, M. Inbar, R. Rosso, E. Grischke, A. Santoro, R. Catane, D.G. Kieback, P. Tomczak, S.P. Ackland, F. Orlandi, L. Mellars, L. Alland, C. Tendler, C.B.C.S. Group, Reduced cardiotoxicity and comparable efficacy in a phase IIItrial of pegylated liposomal doxorubicin HCl(CAELYXTM/Doxil®) versus conventional doxorubicin forfirst-line treatment of metastatic breast cancer, Ann. Oncol. 15 (2004) 440–449, https://doi.org/10.1093/annonc/mdh097

[3] T.J. Anchordoquy, Y. Barenholz, D. Boraschi, M. Chorny, P. Decuzzi, M.A. Dobrovolskaia, Z.S. Farhangrazi, D. Farrell, A. Gabizon, H. Ghandehari, B. Godin, N.M. La-Beck, J. Ljubimova, S.M. Moghimi, L. Pagliaro, J.H. Park, D. Peer, E. Ruoslahti, N.J. Serkova, D. Simberg, Mechanisms and barriers in cancer nanomedicine: addressing challenges, looking for solutions, ACS Nano 11 (2017) 12–18, https://doi.org/10.1021/acsnano.6b08244

[4] U. Prabhakar, H. Maeda, R.K. Jain, E.M. Sevick-Muraca, W. Zamboni, O.C. Farokhzad, S.T. Barry, A. Gabizon, P. Grodzinski, D.C. Blakey, Challenges and key considerations of the enhanced permeability and retention effect for nanomedicine drug delivery in oncology, Cancer Res. 73 (2013) 2412–2417, https://doi.org/10.1158/0008-5472.CAN-12-4561

[5] F. Danhier, To exploit the tumor microenvironment: since the EPR effect fails in the clinic, what is the future of nanomedicine, J. Control. Release 244 (2016) 108–121, https://doi.org/10.1016/j.jconrel.2016.11.015

[6] N.A. Fonseca, A.C. Gregorio, A. Valerio-Fernandes, S. Simoes, J.N. Moreira, Bridging cancer biology and the patients' needs with nanotechnology-based approaches, Cancer Treat. Rev. 40 (2014) 626–635, https://doi.org/10.1016/j.ctrv.2014.02.002

[7] J.W. Park, K. Hong, D.B. Kirpotin, G. Colbern, R. Shalaby, J. Baselga, Y. Shao, U.B. Nielsen, J.D. Marks, D. Moore, D. Papahadjopoulos, C.C. Benz, Clin. Cancer Res. 8 (2002) 1172–1181 https://doi.org/https://clincancerres.aacrjournals.org/content/8/4/1172.long.

[8] K. Miller, J. Cortes, S.A. Hurvitz, I.E. Krop, D. Tripathy, S. Verma, K. Riahi, J.G. Reynolds, T.J. Wickham, I. Molnar, D.A. Yardley, HERMIONE: a randomized Phase 2 trial of MM-302 plus trastuzumab versus chemotherapy of physician's choice plus trastuzumab in patients with previously treated, anthracycline-naïve, HER2-positive, locally advanced/metastatic breast cancer, BMC Cancer 16 (2016) 352, https://doi.org/10.1186/s12885-016-2385-z

[9] S. Sindhwani, A.M. Syed, J. Ngai, B.R. Kingston, L. Maiorino, J. Rothschild, P. MacMillan, Y. Zhang, N.U. Rajesh, T. Hoang, J.L.Y. Wu, S. Wilhelm, A. Zilman, S. Gadde, A. Sulaiman, B. Ouyang, Z. Lin, L. Wang, M. Egeblad, W.C.W. Chan, The entry of nanoparticles into solid tumours, Nat. Mater. 19 (2020) 566–575, https://doi.org/10.1038/s41563-019-0566-2

[10] C.M. Berger, X. Gaume, P. Bouvet, The roles of nucleolin subcellular localization in cancer, Biochimie 113 (2015) 78–85, https://doi.org/10.1016/j.biochi.2015.03.023

[11] J.Y. Xu, S. Lu, X.Y. Xu, S.L. Hu, B. Li, W.X. Li, J.Y. Chang, Tumour Biol. 37 (2016) 10349–10356, https://doi.org/10.1007/s13277-016-4920-6

[12] W. Qiu, F. Zhou, Q. Zhang, X. Sun, X. Shi, Y. Liang, X. Wang, L. Yue, Overexpression of nucleolin and different expression sites both related to the prognosis of gastric cancer, APMIS 121 (2013) 919–925, https://doi.org/10.1111/apm.12131

[13] C. Chen, L. Chen, Y. Yao, Z. Qin, H. Chen, Nucleolin overexpression is associated with an unfavorable outcome for ependymoma: a multifactorial analysis of 176 patients, J. Neurooncol. 127 (2016) 43–52, https://doi.org/10.1007/s11060-015-2007-7

[14] S. Christian, J. Pilch, M.E. Akerman, K. Porkka, P. Laakkonen, E. Ruoslahti, Nucleolin expressed at the cell surface is a marker of endothelial cells in angiogenic blood vessels, J. Cell Biol. 163 (2003) 871–878, https://doi.org/10.1083/jcb.200304132

[15] N.A. Fonseca, A.F. Cruz, V. Moura, S. Simoes, J.N. Moreira, The cancer stem cell phenotype as a determinant factor of the heterotypic nature of breast tumors, Crit. Rev. Oncol. Hematol. 113 (2017) 111–121, https://doi.org/10.1016/j.critrevonc.2017.03.016

[16] V. Moura, M. Lacerda, P. Figueiredo, M.L. Corvo, M.E. Cruz, R. Soares, M.C. de Lima, S. Simoes, J.N. Moreira, Targeted and intracellular triggered delivery of therapeutics to cancer cells and the tumor microenvironment: impact on the treatment of breast cancer, Breast Cancer Res. Treat. 133 (2012) 61–73, https://doi.org/10.1007/s10549-011-1688-7

[17] K.A. Carter, D. Luo, J. Geng, S.T. Stern, J.F. Lovell, Blood interactions, pharmacokinetics, and depth-dependent ablation of rat mammary tumors with photoactivatable, liposomal doxorubicin, Mol. Cancer Ther. 18 (2019) 592–601, https://doi.org/10.1158/1535-7163.MCT-18-0549

[18] T. Terasaki, T. Iga, Y. Sugiyama, M. Hanano, Pharmacokinetic study on the mechanism of tissue distribution of doxorubicin: interorgan and interspecies variation of tissue-to-plasma partition coefficients in rats, rabbits, and guinea pigs, J. Pharm. Sci. 73 (1984) 1359–1363, https://doi.org/10.1002/jps.2600731008

[19] P.K. Working, A.D. Dayan, Hum. Exp. Toxicol. 15 (1996) 751–785, https://doi.org/10.1177/096032719601500906

[20] A. Mathers, G.O. Evans, J. Bleby, Reticulocyte measurements in rat, dog and mouse whole blood samples using the Sysmex XT-2000iV, Comp. Clin. Pathol. 21 (2011) 631–637, https://doi.org/10.1007/s00580-010-1147-6

[21] S.Y. Choi, J.S. Hwang, I.H. Kim, D.Y. Hwang, H.G. Kang, Basic data on the hematology, serum biochemistry, urology, and organ weights of beagle dogs, Lab. Anim. Res. 27 (2011) 283–291, https://doi.org/10.5625/lar.2011.27.4.283

[22] P.J. O'Brien, D.E. Smith, T.J. Knechtel, M.A. Marchak, I. Pruimboom-Brees, D.J. Brees, D.P. Spratt, F.J. Archer, P. Butler, A.N. Potter, J.P. Provost, J. Richard, P.A. Snyder, W.J. Reagan, Cardiac troponin I is a sensitive, specific biomarker of cardiac injury in laboratory animals, Lab. Anim. 40 (2006) 153–171, https://doi.org/10.1258/002367706776319042

[23] J.M. Rae, C.J. Creighton, J.M. Meck, B.R. Haddad, M.D. Johnson, MDA-MB-435 cells are derived from M14 Melanoma cells––a loss for breast cancer, but a boon for melanoma research, Breast Cancer Res. Treat. 104 (2007) 13–19, https://doi.org/10.1007/s10549-006-9392-8

[24] S. Sellappan, R. Grijalva, X. Zhou, W. Yang, M.B. Eli, G.B. Mills, D. Yu, Lineage infidelity of MDA-MB-435 cells: expression of melanocyte proteins in a breast cancer cell line, Cancer Res. 64 (2004) 3479–3485, https://doi.org/10.1158/0008-5472.CAN-3299-2

[25] S. Reagan-Shaw, M. Nihal, N. Ahmad, Dose translation from animal to human studies revisited, FASEB J. 22 (2008) 659–661, https://doi.org/10.1096/fj.07-9574LSF

[26] A. Maksimenko, F. Dosio, J. Mougin, A. Ferrero, S. Wack, L.H. Reddy, A.A. Weyn, E. Lepeltier, C. Bourgaux, B. Stella, L. Cattel, P. Couvreur, A unique squalenoylated and nonpegylated doxorubicin nanomedicine with systemic long-circulating properties and anticancer activity, Proc. Natl. Acad. Sci. USA 111 (2014) E217–226, https://doi.org/10.1073/pnas.1313459110

[27] A.C. Eriksen, J.B. Andersen, M. Kristensson, R. dePont Christensen, T.F. Hansen, S. Kjaer-Frifeldt, F.B. Sorensen, Computer-assisted stereology and automated image analysis for quantification of tumor infiltrating lymphocytes in colon cancer, Diagn. Pathol. 12 (2017) 65, https://doi.org/10.1186/s13000-017-0653-0

[28] G.S. Duncan, D.P. Andrew, H. Takimoto, S.A. Kaufman, H. Yoshida, J. Spellberg, J.L. de la Pompa, A. Elia, A. Wakeham, B. Karan-Tamir, W.A. Muller, G. Senaldi, M.M. Zukowski, T.W. Mak, J. Immunol. 162 (1999) 3022–3030 https://doi.org/https://www.jimmunol.org/content/162/5/3022.

[29] T. Teesalu, K.N. Sugahara, V.R. Kotamraju, E. Ruoslahti, C-end rule peptides mediate neuropilin-1-dependent cell, vascular, and tissue penetration, Proc. Natl. Acad. Sci. USA 106 (2009) 16157–16162, https://doi.org/10.1073/pnas.0908201106

[30] L.T. Senbanjo, M.A. Chellaiah, CD44: A multifunctional cell surface adhesion receptor is a regulator of progression and metastasis of cancer cells, Front. Cell Dev. Biol. 5 (2017) 18, https://doi.org/10.3389/fcell.2017.00018

[31] M.E. Losfeld, D.E. Khoury, P. Mariot, M. Carpentier, B. Krust, J.P. Briand, J. Mazurier, A.G. Hovanessian, D. Legrand, The cell surface expressed nucleolin is a glycoprotein that triggers calcium entry into mammalian cells, Exp. Cell Res. 315 (2009) 357–369, https://doi.org/10.1016/j.yexcr.2008.10.039

[32] E. Barone, F. Gemignani, S. Landi, Overexpressed genes in malignant pleural mesothelioma: implications in clinical management, J. Thorac. Dis. 10 (2018) S369–S382, https://doi.org/10.21037/jtd.2017.10.158

[33] S.E. Chen, M.B. Pace, Malignant pleural mesothelioma, Am. J. Health Syst. Pharm. AJHP Off. J. Am. Soc. Health Syst. Pharm. 69 (2012) 377–385, https://doi.org/10.2146/ajhp110281

[34] H. Saadi, M. Seillier, A. Carrier, The stress protein TP53INP1 plays a tumor suppressive role by regulating metabolic homeostasis, Biochimie 118 (2015) 44–50, https://doi.org/10.1016/j.biochi.2015.07.024

[35] D.A. Vargas, S. Takahashi, Z. Ronai, Mdm2: A regulator of cell growth and death, Adv. Cancer Res. 89 (2003) 1–34, https://doi.org/10.1016/s0065-230x(03)01001-7

[36] Y. Haupt, R. Maya, A. Kazaz, M. Oren, Mdm2 promotes the rapid degradation of p53, Nature 387 (1997) 296–299, https://doi.org/10.1038/387296a0

[37] F. Nguyen Van Long, A. Lardy-Cleaud, S. Bray, S. Chabaud, T. Dubois, A. Diot, A.M. Thompson, J.C. Bourdon, D. Perol, P. Bouvet, J.J. Diaz, V. Marcel, Druggable nucleolin identifies breast tumours associated with poor prognosis that exhibit different biological processes, Cancers 10 (2018) 390, https://doi.org/10.3390/cancers10100390

[38] C. Desmedt, F. Piette, S. Loi, Y. Wang, F. Lallemand, B. Haibe-Kains, G. Viale, M. Delorenzi, Y. Zhang, M.S. d'Assignies, J. Bergh, R. Lidereau, P. Ellis, A.L. Harris, J.G. Klijn, J.A. Foekens, F. Cardoso, M.J. Piccart, M. Buyse, C. Sotiriou, T. Consortium, Strong time dependence of the 76-gene prognostic signature for node-negative breast cancer patients in the TRANSBIG multicenter independent validation series, Clin. Cancer Res. 13 (2007) 3207–3214, https://doi.org/10.1158/1078-0432.CCR-06-2765

[39] Y. Wang, J.G.M. Klijn, Y. Zhang, A.M. Sieuwerts, M.P. Look, F. Yang, D. Talantov, M. Timmermans, M.E. Meijer-van Gelder, J. Yu, T. Jatkoe, E.M.J.J. Berns, D. Atkins, J.A. Foekens, Gene-expression profiles to predict distant metastasis of lymph-node-negative primary breast cancer, Lancet 365 (2005) 671–679, https://doi.org/10.1016/s0140-6736(05)70933-8

[40] G.J. Gordon, G.N. Rockwell, R.V. Jensen, J.G. Rheinwald, J.N. Glickman, J.P. Aronson, B.J. Pottorf, M.D. Nitz, W.G. Richards, D.J. Sugarbaker, R. Bueno, Identification of novel candidate oncogenes and tumor suppressors in malignant pleural mesothelioma using large-scale transcriptional profiling, Am. J. Pathol. 166 (2005) 1827–1840, https://doi.org/10.1016/s0002-9440(10)62492-3

[41] Y. Barenholz, Doxil® — The first FDA-approved nano-drug: lessons learned, J. Control. Release 160 (2012) 117–134, https://doi.org/10.1016/j.jconrel.2012.03.020

[42] S. Wilhelm, A.J. Tavares, Q. Dai, S. Ohta, J. Audet, H.F. Dvorak, W.C.W. Chan, Analysis of nanoparticle delivery to tumours, Nat. Rev. Mater. 1 (2016) 16014, https://doi.org/10.1038/natrevmats.2016.14

[43] B.S. Zolnik, N. Sadrieh, Regulatory perspective on the importance of ADME assessment of nanoscale material containing drugs, Adv. Drug Deliv. Rev. 61 (2009) 422–427, https://doi.org/10.1016/j.addr.2009.03.006

[44] T. Ishida, M.J. Kirchmeier, E.H. Moase, S. Zalipsky, T.M. Allen, Targeted delivery and triggered release of liposomal doxorubicin enhances cytotoxicity against human B lymphoma cells, Biochim. Biophys. Acta (BBA) Biomembr. 1515 (2001) 144–158, https://doi.org/10.1016/S0005-2736(01)00409-6

[45] V.A. Slepushkin, S. Simoes, P. Dazin, M.S. Newman, L.S. Guo, M.C. Pedroso de Lima, N. Duzgunes, Sterically stabilized pH-sensitive liposomes, intracellular delivery of aqueous contents and prolonged circulation in vivo, J. Biol. Chem. 272 (1997) 2382–2388, https://doi.org/10.1074/jbc.272.4.2382

[46] P.P. Wibroe, D. Ahmadvand, M.A. Oghabian, A. Yaghmur, S.M. Moghimi, An integrated assessment of morphology, size, and complement activation of the PEGylated liposomal doxorubicin products Doxil®, Caelyx®, DOXOrubicin, and SinaDoxosome, J. Control. Release 221 (2016) 1–8, https://doi.org/10.1016/j.jconrel.2015.11.021

[47] S. Bhattacharjee, DLS and zeta potential – what they are and what they are not, J. Control. Release 235 (2016) 337–351, https://doi.org/10.1016/j.jconrel.2016.06.017

[48] R. Michel, M. Gradzielski, Experimental aspects of colloidal interactions in mixed systems of liposome and inorganic nanoparticle and their applications, Int. J. Mol. Sci. 13 (2012) 11610–11642, https://doi.org/10.3390/ijms130911610

[49] J.M. Rabanel, P. Hildgen, X. Banquy, Assessment of PEG on polymeric particles surface, a key step in drug carrier translation, J. Control. Release 185 (2014) 71–87, https://doi.org/10.1016/j.jconrel.2014.04.017

[50] H. Kouchakzadeh, S.A. Shojaosadati, A. Maghsoudi, E. Vasheghani Farahani, Optimization of PEGylation conditions for BSA nanoparticles using response surface methodology, AAPS PharmSciTech 11 (2010) 1206–1211, https://doi.org/10.1208/s12249-010-9487-8

[51] G. Pearse, Histopathology of the thymus, Toxicol. Pathol. 34 (2006) 515–547, https://doi.org/10.1080/01926230600978458

[52] Y. Octavia, C.G. Tocchetti, K.L. Gabrielson, S. Janssens, H.J. Crijns, A.L. Moens, Doxorubicin-induced cardiomyopathy: from molecular mechanisms to therapeutic strategies, J. Mol. Cell. Cardiol. 52 (2012) 1213–1225, https://doi.org/10.1016/j.yjmcc.2012.03.006

[53] G. Minotti, P. Menna, E. Salvatorelli, G. Cairo, L. Gianni, Anthracyclines: molecular advances and pharmacologic developments in antitumor activity and cardiotoxicity, Pharmacol. Rev. 56 (2004) 185–229, https://doi.org/10.1124/pr.56.2.6

[54] P. Greaves, Histopathology of Preclinical Toxicity Studies, fourth ed., 2012, pp. 615–666. ⟨https://doi.org/10.1016/B978-0-444-53856-7.00011-7⟩.

[55] J. Cui, C. Li, W. Guo, Y. Li, C. Wang, L. Zhang, L. Zhang, Y. Hao, Y. Wang, Direct comparison of two pegylated liposomal doxorubicin formulations: is AUC predictive for toxicity and efficacy, J. Control. Release 118 (2007) 204–215, https://doi.org/10.1016/j.jconrel.2006.12.002

[56] D.B. Kirpotin, D.C. Drummond, Y. Shao, M.R. Shalaby, K. Hong, U.B. Nielsen, J.D. Marks, C.C. Benz, J.W. Park, Antibody targeting of long-circulating lipidic nanoparticles does not increase tumor localization but does increase internalization in animal models, Cancer Res. 66 (2006) 6732–6740, https://doi.org/10.1158/0008-5472.CAN-05-4199

[57] D. Destouches, D. El Khoury, Y. Hamma-Kourbali, B. Krust, P. Albanese, P. Katsoris, G. Guichard, J.P. Briand, J. Courty, A.G. Hovanessian, Suppression of tumor growth and angiogenesis by a specific antagonist of the cell-surface expressed nucleolin, PLoS One 3 (2008) e2518, https://doi.org/10.1371/journal.pone.0002518

[58] E.A. Said, J. Courty, J. Svab, J. Delbe, B. Krust, A.G. Hovanessian, Pleiotrophin inhibits HIV infection by binding the cell surface-expressed nucleolin, FEBS J. 272 (2005) 4646–4659, https://doi.org/10.1111/j.1742-4658.2005.04870.x

[59] E.A. Said, B. Krust, S. Nisole, J. Svab, J.P. Briand, A.G. Hovanessian, The anti-HIV cytokine midkine binds the cell surface-expressed nucleolin as a low affinity receptor, J. Biol. Chem. 277 (2002) 37492–37502, https://doi.org/10.1074/jbc.M201194200

[60] S. Nisole, B. Krust, A.G. Hovanessian, Anchorage of HIV on permissive cells leads to coaggregation of viral particles with surface nucleolin at membrane raft microdomains, Exp. Cell Res. 276 (2002) 155–173, https://doi.org/10.1006/excr.2002.5522

[61] J.W. Nichols, Y.H. Bae, EPR: Evidence and fallacy, J. Control. Release 190 (2014) 451–464, https://doi.org/10.1016/j.jconrel.2014.03.057

[62] R. Vazquez, S.A. Licandro, L. Astorgues-Xerri, E. Lettera, N. Panini, M. Romano, E. Erba, P. Ubezio, E. Bello, R. Libener, S. Orecchia, F. Grosso, M.E. Riveiro, E. Cvitkovic, M. Bekradda, M. D'Incalci, R. Frapolli, Promisingin vivoefficacy of the BET bromodomain inhibitor OTX015/MK-8628 in malignant pleural mesothelioma xenografts: OTX015 Activity IN MPM, Int. J. Cancer 140 (2017) 197–207, https://doi.org/10.1002/ijc.30412

[63] C. Pisano, A.G. Cole, M. Barbarino, E. Bianchino, M. Guglielmi, C. Melito, G. Mercadante, A. Porciello, A. Riccio, I.L. Porta, S. Orecchia, R. Libener, L. Mazzucco, S.A. Licandro, P.D. Luca, Cancer Res. 74 (2014) 5556, https://doi.org/10.1158/1538-7445.am2014-5556

[64] F. Li, J. Lu, J. Liu, C. Liang, M. Wang, L. Wang, D. Li, H. Yao, Q. Zhang, J. Wen, Z.K. Zhang, J. Li, Q. Lv, X. He, B. Guo, D. Guan, Y. Yu, L. Dang, X. Wu, Y. Li, G. Chen, F. Jiang, S. Sun, B.T. Zhang, A. Lu, G. Zhang, A water-soluble nucleolin aptamer-paclitaxel conjugate for tumor-specific targeting in ovarian cancer, Nat. Commun. 8 (2017) 1390, https://doi.org/10.1038/s41467-017-01565-6

[65] K. Porpodis, P. Zarogoulidis, E. Boutsikou, A. Papaioannou, N. Machairiotis, K. Tsakiridis, N. Katsikogiannis, B. Zaric, B. Perin, H. Huang, I. Kougioumtzi, D. Spyratos, K. Zarogoulidis, J. Thorac. Dis. 5 Suppl 4 (2013) S397–406, https://doi.org/10.3978/j.issn.2072-1439.2013.08.08

[66] F. Berrino, R. De Angelis, M. Sant, S. Rosso, M.B. Lasota, J.W. Coebergh, M. Santaquilani, Survival for eight major cancers and all cancers combined for European adults diagnosed in 1995–99: results of the EUROCARE-4 study, Lancet Oncol. 8 (2007) 773–783, https://doi.org/10.1016/s1470-2045(07)70245-0

[67] D.J. Erstad, M. Sojoodi, M.S. Taylor, V.C. Jordan, C.T. Farrar, A.L. Axtell, N.J. Rotile, C. Jones, K.A. Graham-O'Regan, D.S. Ferreira, T. Michelakos, F. Kontos, A. Chawla, S. Li, S. Ghoshal, Y.I. Chen, G. Arora, V. Humblet, V. Deshpande, M. Qadan, N. Bardeesy, C.R. Ferrone, M. Lanuti, K.K. Tanabe, P. Caravan, B.C. Fuchs, Fibrotic response to neoadjuvant therapy predicts survival in pancreatic cancer and is measurable with collagen-targeted molecular MRI, Clin. Cancer Res. 26 (2020) 5007–5018, https://doi.org/10.1158/1078-0432.CCR-18-1359

[68] P. Schmid, S. Adams, H.S. Rugo, A. Schneeweiss, C.H. Barrios, H. Iwata, V. Dieras, R. Hegg, S.A. Im, G. Shaw Wright, V. Henschel, L. Molinero, S.Y. Chui, R. Funke, A. Husain, E.P. Winer, S. Loi, L.A. Emens, I.M.T. Investigators, Atezolizumab and Nab-paclitaxel in advanced triple-negative breast cancer, N. Engl. J. Med. 379 (2018) 2108–2121, https://doi.org/10.1056/NEJMoa1809615

[69] J.P.H. Machiels, R.T. Reilly, L.A. Emens, A. Ercolini, R.Y. Lei, D. Weintraub, F.I. Okoye, E.M. Jaffee, Cancer Res. 61 (2001) 3689–3697.

[70] Y. Ma, L. Galluzzi, L. Zitvogel, G. Kroemer, Autophagy and cellular immune responses, Immunity 39 (2013) 211–227, https://doi.org/10.1016/j.immuni.2013.07.017

[71] N.A. Fonseca, L.C. Gomes-da-Silva, V. Moura, S. Simoes, J.N. Moreira, Simultaneous active intracellular delivery of doxorubicin and C6-ceramide shifts the additive/antagonistic drug interaction of non-encapsulated combination, J. Control. Release 196 (2014) 122–131, https://doi.org/10.1016/j.jconrel.2014.09.024

[72] N.A. Fonseca, A.S. Rodrigues, P. Rodrigues-Santos, V. Alves, A.C. Gregorio, A. Valerio-Fernandes, L.C. Gomes-da-Silva, M.S. Rosa, V. Moura, J. Ramalho-Santos, S. Simoes, J.N. Moreira, Nucleolin overexpression in breast cancer cell sub-populations with different stem-like phenotype enables targeted intracellular delivery of synergistic drug combination, Biomaterials 69 (2015) 76–88, https://doi.org/10.1016/j.biomaterials.2015.08.007

[73] N.J. Vogelzang, J.J. Rusthoven, J. Symanowski, C. Denham, E. Kaukel, P. Ruffie, U. Gatzemeier, M. Boyer, S. Emri, C. Manegold, C. Niyikiza, P. Paoletti, Phase III study of pemetrexed in combination with cisplatin versus cisplatin alone in patients with malignant pleural mesothelioma, J. Clin. Oncol. 21 (2003) 2636–2644, https://doi.org/10.1200/JCO.2003.11.136

[74] M.P. Kai, A.W. Keeler, J.L. Perry, K.G. Reuter, J.C. Luft, S.K. O'Neal, W.C. Zamboni, J.M. DeSimone, Evaluation of drug loading, pharmacokinetic behavior, and toxicity of a cisplatin-containing hydrogel nanoparticle, J. Control. Release 204 (2015) 70–77, https://doi.org/10.1016/j.jconrel.2015.03.001

[75] B.S. Carvalho, R.A. Irizarry, A framework for oligonucleotide microarray preprocessing, Bioinformatics 26 (2010) 2363–2367, https://doi.org/10.1093/bioinformatics/btq431

[76] R.A. Irizarry, B. Hobbs, F. Collin, Y.D. Beazer-Barclay, K.J. Antonellis, U. Scherf, T.P. Speed, Exploration, normalization, and summaries of high density oligonucleotide array probe level data, Biostatistics 4 (2003) 249–264, https://doi.org/10.1093/biostatistics/4.2.249

[77] B.M. Bolstad, R.A. Irizarry, M. Astrand, T.P. Speed, A comparison of normalization methods for high density oligonucleotide array data based on variance and bias, Bioinformatics 19 (2003) 185–193, https://doi.org/10.1093/bioinformatics/19.2.185

[78] M.E. Ritchie, B. Phipson, D. Wu, Y. Hu, C.W. Law, W. Shi, G.K. Smyth, limma powers differential expression analyses for RNA-sequencing and microarray studies, Nucleic Acids Res. 43 (2015) e47, https://doi.org/10.1093/nar/gkv007

[79] T. Barrett, S.E. Wilhite, P. Ledoux, C. Evangelista, I.F. Kim, M. Tomashevsky, K.A. Marshall, K.H. Phillippy, P.M. Sherman, M. Holko, A. Yefanov, H. Lee, N. Zhang, C.L. Robertson, N. Serova, S. Davis, A. Soboleva, NCBI GEO: archive for functional genomics data sets—update, Nucleic Acids Res. 41 (2012) D991–995, https://doi.org/10.1093/nar/gks1193

[80] Z. Gu, R. Eils, M. Schlesner, Complex heatmaps reveal patterns and correlations in multidimensional genomic data, Bioinformatics 32 (2016) 2847–2849, https://doi.org/10.1093/bioinformatics/btw313

[81] M. Krzywinski, J. Schein, I. Birol, J. Connors, R. Gascoyne, D. Horsman, S.J. Jones, M.A. Marra, Circos: An information aesthetic for comparative genomics, Genome Res. 19 (2009) 1639–1645, https://doi.org/10.1101/gr.092759.109